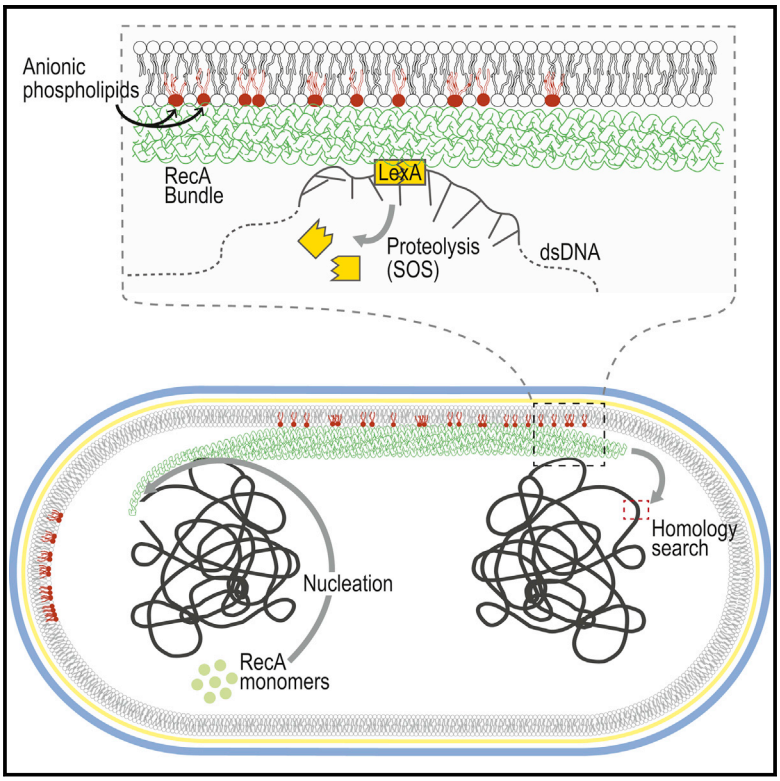
Article

Molecular Cell

Anionic Phospholipids Stabilize RecA Filament Bundles in *Escherichia coli*

Graphical Abstract



Highlights

- Phosphatidylglycerol (PG) and cardiolipin (CL) interact with *Escherichia coli* RecA
- In vitro ATPase activity is inhibited in the presence of PG and CL
- RecA foci mislocalize in the absence of PG and CL in vivo
- RecA bundle morphology and SOS response are affected in the absence of PG and CL

Authors

Manohary Rajendram, Leili Zhang, Bradley J. Reynolds, ..., Arun Yethiraj, Qiang Cui, Douglas B. Weibel

Correspondence

weibel@biochem.wisc.edu

In Brief

Using 3D-structured illumination microscopy, Rajendram et al. show that anionic phospholipids of the inner membrane provide a scaffold for the formation of RecA filament bundles, aid in DNA repair, and facilitate the DNA damage response in *Escherichia coli*.

Rajendram et al., 2015, Molecular Cell *60*, 374–384
November 5, 2015 ©2015 Elsevier Inc.
http://dx.doi.org/10.1016/j.molcel.2015.09.009

CrossMark

CellPress

CellPress

Molecular Cell
Article

Anionic Phospholipids Stabilize RecA Filament Bundles in *Escherichia coli*

Manohary Rajendram,[1] Leili Zhang,[2,3] Bradley J. Reynolds,[1] George K. Auer,[4] Hannah H. Tuson,[1] Khanh V. Ngo,[1] Michael M. Cox,[1] Arun Yethiraj,[2,3] Qiang Cui,[2,3] and Douglas B. Weibel[1,2,4,*]
[1]Department of Biochemistry, University of Wisconsin-Madison, Madison, WI 53706, USA
[2]Department of Chemistry, University of Wisconsin-Madison, Madison, WI 53706, USA
[3]Theoretical Chemistry Institute, University of Wisconsin-Madison, Madison, WI 53706, USA
[4]Department of Biomedical Engineering, University of Wisconsin-Madison, Madison, WI 53706, USA
*Correspondence: weibel@biochem.wisc.edu
http://dx.doi.org/10.1016/j.molcel.2015.09.009

SUMMARY

We characterize the interaction of RecA with membranes in vivo and in vitro and demonstrate that RecA binds tightly to the anionic phospholipids cardiolipin (CL) and phosphatidylglycerol (PG). Using computational models, we identify two regions of RecA that interact with PG and CL: (1) the N-terminal helix and (2) loop L2. Mutating these regions decreased the affinity of RecA to PG and CL in vitro. Using 3D super-resolution microscopy, we demonstrate that depleting *Escherichia coli* PG and CL altered the localization of RecA foci and hindered the formation of RecA filament bundles. Consequently, *E. coli* cells lacking aPLs fail to initiate a robust SOS response after DNA damage, indicating that the membrane acts as a scaffold for nucleating the formation of RecA filament bundles and plays an important role in the SOS response.

INTRODUCTION

RecA repairs DNA damage by performing homologous recombination and is the primary mediator of the DNA damage (SOS) response in *Escherichia coli*. RecA binds ATP; polymerizes on exposed, single-stranded DNA (ssDNA); and creates nucleoprotein filaments that facilitate DNA repair through a mechanism that entails homology searching and matching of complementary strands. RecA nucleoprotein filaments subsequently cleave the LexA repressor and initiate the SOS response leading to the downstream transcription of ~40 genes that facilitate DNA repair. After the process of DNA repair is complete, RecA filaments hydrolyze ATP and dissociate from DNA.

A translational fusion of green fluorescent protein (GFP) to the C terminus of RecA (RecA-GFP) localizes into polar foci in *E. coli* (Renzette et al., 2005). These foci, referred to as storage structures, are reminiscent of the RecA aggregates observed in vitro (Brenner et al., 1988; Story et al., 1992). These foci do not form in RecA mutants unable to bind ATP, highlighting the importance of the ATP-bound form of RecA in the stability of these aggregates and mirroring observations from in vitro studies (Brenner et al., 1988; Egelman and Stasiak, 1988). When DNA is damaged, RecA-GFP redistributes from foci into long filament-like structures that span the chromosome and are referred to as bundles (Lesterlin et al., 2014; Renzette and Sandler, 2008). Lesterlin et al. demonstrated that these laterally associated bundles of RecA filaments that extend from the site of a double-stranded DNA break (DSB) assemble along the length of the cell in a step that appears to be connected to the search for DNA sequence homology. These bundles have been observed in vivo in *E. coli* by electron microscopy (Levin-Zaidman et al., 2000). Interestingly, the majority of RecA protein within these bundles (hereafter referred to as filament bundles) appears to not be associated with DNA (Lesterlin et al., 2014). They are occluded from the nucleoid and positioned close to the inner membrane (IM), suggesting the possibility of membrane-RecA interactions during DNA repair. The association of RecA with membranes during SOS was reported nearly three decades ago in *E. coli* lysates (Garvey et al., 1985), and yet very little is known about this interaction (Papanastasiou et al., 2013), its relevance to RecA location and function, and its role in cell physiology.

In this study, we test the hypothesis that the interaction of RecA with membranes is important for its activity in vivo. We use experimental and computational methods to characterize the binding of RecA to anionic phospholipids (aPLs), identify the RecA interfaces responsible, and demonstrate that this interaction decreases the ATPase activity of RecA in vitro. Further, we observe that RecA is mislocalized in *E. coli* mutants unable to produce aPLs and the SOS response in these mutants is significantly reduced. We show that the formation of RecA filament bundles is decreased in mutants lacking aPLs and this impairment in filament bundle formation hinders the progress of the SOS response. Our results indicate that aPLs stabilize polarly localized storage forms of RecA and provide a scaffold for the formation of RecA filament bundles that facilitate the SOS response after DNA damage. These observations provide a context for the physiological significance of RecA-membrane interactions in *E. coli* and highlight an important role of the IM in the cellular response to DNA damage.

RESULTS

RecA Binds aPLs In Vitro

To determine the affinity of RecA to PLs, we purified recombinant RecA from *E. coli* and measured the affinity of RecA to

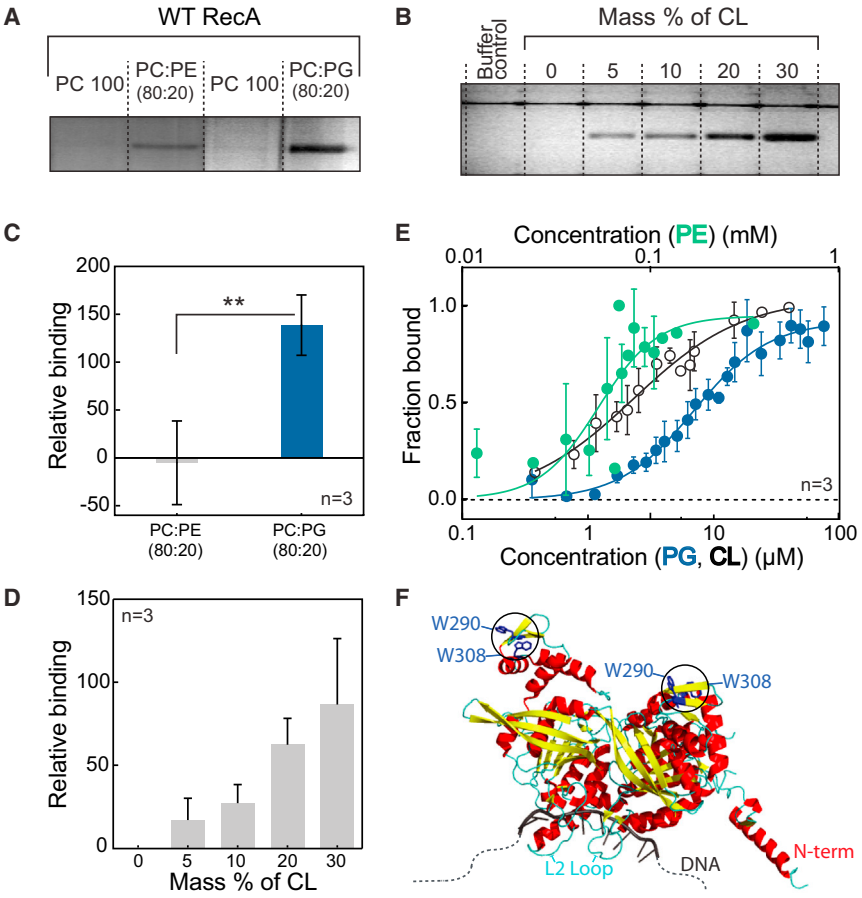


Figure 1. *E. coli* RecA Interacts Specifically and with High Affinity to Anionic Phospholipids

(A and C) Co-flotation assays of RecA with PE and PG demonstrate that RecA binds to anionic PLs with high affinity. **$p < 0.05$ indicates statistical significance calculated by a two-tailed t test.

(B and D) The binding of RecA with CL increases proportionally with increasing CL concentration.

(E) Langmuir binding isotherms of RecA with PE, PG, and CL demonstrate binding parameters as follows: PE (K_d = 52.9 ± 8.6 μM, Hill coefficient = 2.8 ± 1.1 and R^2 = 0.7), PG (K_d = 6.9 ± 1.2 μM, Hill coefficient = 1.5 ± 0.3 and R^2 = 0.93), and CL (K_d = 2.4 ± 0.4 μM, Hill coefficient = 1.0 ± 0.1 and R^2 = 0.91).

(F) Crystal structure (PDB: 3CMU) of a dimer of RecA showing the position of the two Trp residues used to quantify binding affinities. All error bars indicate SD.

zwitterionic PLs (phosphatidylethanolamine [PE], phosphatidylcholine [PC]) and aPLs (phosphatidylglycerol [PG], cardiolipin [CL]) using liposome co-floatation assays. We quantified the amount of *E. coli* RecA that floats with liposomes and found that RecA displays a specific and high-affinity interaction with the aPLs, PG and CL (Figures 1A–1D) and a weaker association with PE (all found in *E. coli* IM), but no association with PC (not found in *E. coli* IM).

We quantitatively determined apparent dissociation constants (K_ds) for PG, CL, and PE by using the inherent fluorescence of tryptophans (Trp) at positions 290 and 309 in RecA (Figure 1F). The fluorescence intensity and wavelength of maximum emission of Trp residues reflect changes in the chemical microenvironment within proteins (Vivian and Callis, 2001) that may arise in response to protein-membrane binding events and can be used to quantify these interactions. We found the interaction of RecA with PG-, CL-, and PE-containing liposomes is coupled to a change in the environment around the Trps that alters the intensity of their fluorescence emission. By titrating in different concentrations of aPLs and fitting the change in Trp fluorescence intensity to a Langmuir isotherm, we determined apparent K_ds for RecA binding to PE (53 μM), PG (7 μM), and CL (2.5 μM) (Figure 1E). Remarkably, the values for PG and CL are within an order of magnitude of the K_d of RecA to ssDNA (0.8–2.5 μM) reported by others (Britt et al., 2011; Menetski and Kowalczykowski, 1985) and measured by us (0.7 μM; Figures S3B and S3D). This high-affinity interaction of RecA to PG and CL suggests that RecA may spend a significant proportion of time on the IM when not bound to ssDNA.

Molecular Dynamics Simulations Identify Key Membrane-Binding Interfaces in RecA

To predict the binding orientation, depth of insertion, and affinity of RecA to the membrane, we combined implicit and explicit membrane simulations. Explicit membrane simulations describe protein/solvent/lipid interactions at an atomistic level and are generally more accurate; however, these simulations are too computationally expensive for binding free energy calculations that involve a relatively large protein such as RecA and are not suited for identifying the residues/motifs that are important in membrane binding. Our strategy was to start with implicit membrane simulations and test the predicted binding conformations further using explicit membrane simulations. Implicit membrane simulations can be used to compute semiquantitative binding free energies and predict the effect of mutations on binding, which can be tested experimentally.

We collected a binding energy map (Figure 2A) using GBSW-GCS and a non-flexible RecA protein and found two low energy configurations. These data are qualitatively consistent with the two binding conformations obtained from flexible MD simulations (Figures 2C and 2D). The binding interfaces of the two binding conformations (Figure 2B) are largely consistent and involve inserting the largely hydrophobic DNA binding loop L2 (I195 to N205) and the N-terminal α-helix, which contains both hydrophobic and charged residues (AIDENKQKAL-N10) into the membrane. Therefore, RecA binding to the anionic membrane involves the interplay of both electrostatic interactions and hydrophobic insertion, which was confirmed further by explicit membrane simulations (Figure S1).

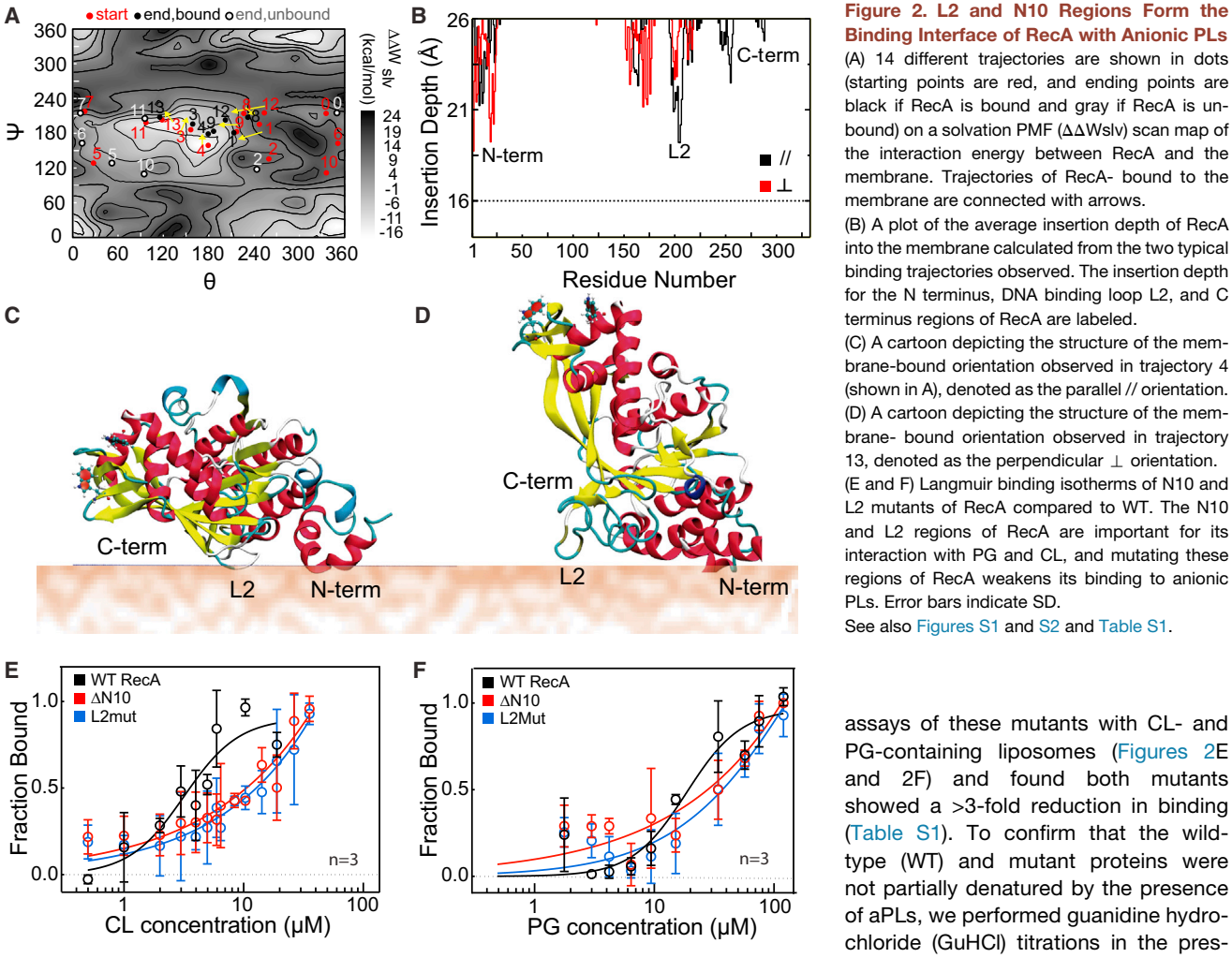


Figure 2. L2 and N10 Regions Form the Binding Interface of RecA with Anionic PLs

(A) 14 different trajectories are shown in dots (starting points are red, and ending points are black if RecA is bound and gray if RecA is unbound) on a solvation PMF (ΔΔWslv) scan map of the interaction energy between RecA and the membrane. Trajectories of RecA- bound to the membrane are connected with arrows.

(B) A plot of the average insertion depth of RecA into the membrane calculated from the two typical binding trajectories observed. The insertion depth for the N terminus, DNA binding loop L2, and C terminus regions of RecA are labeled.

(C) A cartoon depicting the structure of the membrane-bound orientation observed in trajectory 4 (shown in A), denoted as the parallel // orientation.

(D) A cartoon depicting the structure of the membrane- bound orientation observed in trajectory 13, denoted as the perpendicular ⊥ orientation.

(E and F) Langmuir binding isotherms of N10 and L2 mutants of RecA compared to WT. The N10 and L2 regions of RecA are important for its interaction with PG and CL, and mutating these regions of RecA weakens its binding to anionic PLs. Error bars indicate SD.

See also Figures S1 and S2 and Table S1.

Similar to our previous observations, the vertical differential solvation free energies ($\Delta\Delta W_{slv}$) of RecA binding to the membrane correlate with ΔF_{bind} and overestimate this parameter (Zhang et al., 2014). The calculated binding affinity for the parallel binding conformation of RecA to the membrane is substantially stronger than the perpendicular mode by ~5 kcal/mol. We evaluated the parallel and perpendicular conformation for the mutants in which one binding motif (either the N-terminal helix or loop L2) was altered. Our calculations (Table 1) suggest that altering either motif leads to a significant (~50%) reduction in the binding free energy and is qualitatively in agreement with our experimental binding measurements (Figures 2E and 2F and Table S1). The data suggest that both motifs are likely to be involved in binding of RecA to the membrane.

Verification of Membrane-Binding Regions In Vitro

To verify our computational results, we purified two RecA mutants: (1) a mutant lacking the ten N-terminal amino acids (ΔN10), and(2) a mutant containing the substitutions I195A, R196A, K198A, I199A, V201A, and F203A (L2mut); circular dichroism data indicated that both mutants were folded correctly (Figure S2A). We performed Trp fluorescence binding assays of these mutants with CL- and PG-containing liposomes (Figures 2E and 2F) and found both mutants showed a >3-fold reduction in binding (Table S1). To confirm that the wild-type (WT) and mutant proteins were not partially denatured by the presence of aPLs, we performed guanidine hydrochloride (GuHCl) titrations in the presence and absence of 70 μM PG liposomes (~10× the K_d for WT RecA). We observed that all three proteins denatured completely at a GuHCl concentration of 3.75 M. The CD spectra in the presence of PG liposomes showed no significant differences when compared to the spectra in the absence of liposomes and at all GuHCl concentrations tested (Figures S2B–S2D). These results confirm our computational predictions that the N10 and L2 regions contribute significantly to and form the interface for RecA-membrane interactions. The N terminus of RecA has been hypothesized to play a role in the assembly/disassembly of RecA-ssDNA filaments (Mikawa et al., 1995) and the L2 loop is implicated in ssDNA binding and ATPase (Voloshin et al., 2000). Previous work has demonstrated that mutations in both of these regions lead to recombination negative phenotypes in vivo (Table S2). The L2 loop is evolutionarily conserved across many bacterial species (Karlin and Brocchieri, 1996). Interestingly, only four residues within the ten N-terminal amino acids are stringently conserved (K6, K8, A9, and L10). We wondered whether the interaction of RecA with aPLs affects the functions related to these regions' (1) monomer-monomer interactions (ΔN10) and (2) ssDNA binding (L2).

Table 1. Binding Free Energy Calculations Using the GBSW-GCS Model for WT RecA and Mutants to an Anionic Membrane

System[a]	Mutations	$\Delta\Delta W_{slv}$[b]	ΔF_{bind} (kcal/mol)[c]
WT //	–	−21.3 ± 2.3	−9.6 ± 0.9
WT ⊥	–	−13.6 ± 2.3	−5.0 ± 0.5
Mut1 //	Δ10N	−19.2 ± 4.0	−5.3 ± 0.6
Mut1 ⊥	–	−10.8 ± 1.4	−2.3 ± 0.1[d]
Mut2 //	I195A, R196A, K198A, I199A, V201A, F203A	−15.2 ± 6.7	−4.7 ± 2.9
Mut2 ⊥	–	−9.2 ± 1.3	−0.8 ± 0.1

[a]// and ⊥ refer to the parallel and perpendicular binding conformations (see Figures 2C and 2D), respectively.
[b]The vertical differential solvation free energy of the protein at the membrane surface versus in bulk solution. As discussed in Zhang et al., 2014, this quantity correlates with binding free energy when the system does not undergo significant conformational transitions upon binding.
[c]Binding free energy (in kcal/mol) of the protein calculated using the protocol established in Zhang et al., 2014 based on a specific thermodynamic cycle and the Bennett Acceptance Ratio (BAR) approach.
[d]Mut1 for the perpendicular orientation leads to a 1.6 kcal/mol less binding free energy change than the parallel orientation. This is because the weakly perpendicularly bound RecA adjusts Loop L2 insertion to compensate the truncation of N-terminal amino acids to remain as the bound state. Meanwhile, for parallel orientation, the change in insertion depth is negligible.

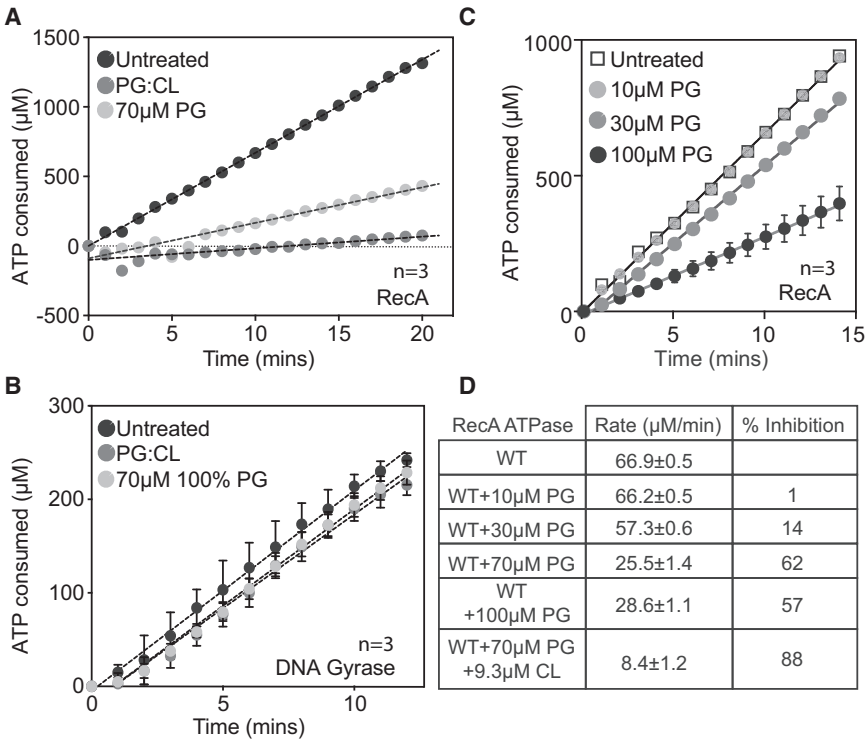
aPLs Inhibit ATPase within RecA Nucleoprotein Filaments

We performed in vitro assays to determine whether interactions with PG/CL perturb RecA binding to ssDNA, strand exchange, and/or ATPase activities. All assays of RecA activity in vitro require Mg^{2+} ions to facilitate ATP binding. The zwitterionic PL, PC, forms a ternary complex with DNA when Mg^{2+} ions are present and confounds results (Kuvichkin et al., 2009). To circumvent this limitation, we avoided the use of PC/PE, and used 100% PG and a mixture of 80% PG+20% CL at 10× the measured K_ds. We measured the DNA-dependent ATPase rate of RecA. We pre-incubated RecA simultaneously with aPLs and ssDNA prior to the addition of ATP to initiate the reaction. This experimental setup enabled us to mimic in vivo conditions where both aPLs and ssDNA (after DNA is damaged) are available simultaneously. We observed that ATPase was inhibited in the presence of CL and PG (Figures 3A and 3D). In identical experimental conditions—controlled for order of addition of different components as well as concentrations of aPLs—we found ssDNA binding to RecA was unaffected (Figures S3A and S3C), and strand exchange progressed to completion (Figures S3E–S3G). We also titrated PG into ATPase reactions to confirm that rates of ATPase decrease as a function of PG concentration (Figures 3C and 3D). This set of experiments revealed four important conclusions: (1) the presence of aPLs did not alter the affinity of RecA to ssDNA, which is consistent with K_d measurements indicating that ssDNA has a higher affinity to RecA than PG or CL; (2) the inhibition of ATPase did not affect the ability of RecA to perform homologous recombination, which is congruent with proposed models that ATPase is required for dissociation of RecA nucleoprotein filaments and is not required for the process of recombination; (3) the reduction in ATPase activity was not due to a reduction in ATP binding, because a decrease in ATP binding would impair strand exchange due to the inability to form RecA filaments; and (4) the RecA protein was not denatured in the presence of aPLs because it remained able to perform DNA strand exchange. To confirm that the effect of aPLs on RecA's ATPase activity is specific, we performed a control experiment with aPLs at identical concentrations with another DNA-dependent ATPase, *E*. coli DNA gyrase (Rajendram et al., 2014). We pre-incubated gyrase with aPLs and DNA prior to the addition of ATP to initiate the reaction. In contrast to RecA, we observed no decrease in ATPase by gyrase when aPLs were present (Figure 3B). These observations indicate that PG and CL produce a specific effect on RecA ATPase but do not alter ATP/DNA binding. We hypothesized that aPLs inhibit dissociation of RecA nucleoprotein filaments by inhibiting ATPase and provide a mechanism for the formation of stable nucleoprotein filaments.

RecA Mislocalizes in the Absence of aPLs

aPLs localize preferentially to the poles of *E. coli* (Oliver et al., 2014; Renner and Weibel, 2011). One hypothesis is that aPLs act as landmarks to recruit proteins to cell poles. Due to the reduction in RecA ATPase in the presence of aPLs, we wondered whether depleting aPLs (*E. coli* BKT29 (Tan et al., 2012)) would alter the localization of RecA-GFP foci that are observed at the *E. coli* poles. Consistent with this hypothesis, previous studies have shown that mutants of RecA (K72A) that do not bind ATP display a decrease in foci formation (Renzette and Sandler, 2008). We transduced RecA-GFP described previously (Renzette et al., 2005) into *E. coli* MG1655 and analyzed RecA-GFP localization and found RecA-GFP foci localized predominantly at the poles (Figures 4A, 4C, and 4D). Approximately 50% of cells had a single focus and ~70% of these cells displayed a unipolar distribution. When multiple foci were present (~5% of cells), at least one focus was present at a pole. Because fluorescent protein tags can cause artifacts in protein localization, we confirmed these results by quantifying the subcellular localization of RecA in *E. coli* using immunofluorescence labeling. We expressed RecA with a C-terminal epitope tag (Xpress DLYDDDDK**)** from a low-copy pBAD plasmid induced with arabinose and quantified foci distribution. We observed a predominantly polar distribution correlating very closely with that of RecA-GFP (Figures 4A and 4F), indicating polarly localized RecA-GFP foci in *E. coli* are not artifacts.

Next, we quantified the localization of RecA-GFP in *E. coli* BKT29 (Figures 4B, 4G–4I) and observed that the distribution of foci was altered, with a >50% reduction in the incidence of polar foci compared to WT cells. Strain *E. coli* BKT29 contains suppressor mutations that stabilize cells depleted of aPLs. To account for the effect of these suppressor mutations, we tested strain *E. coli* UE53, which contains only these mutations, as a background control (Figures S7A and S7E) and found there were no significant differences in RecA localization between UE53 and MG1655. Our observations are consistent with the hypothesis that aPLs stabilize RecA structures at the poles. These foci were not associated with the nucleoid as observed by DAPI staining (Figures 4D and 4I). In contrast, RecA bundles formed in



D

RecA ATPase	Rate (μM/min)	% Inhibition
WT	66.9±0.5	
WT+10μM PG	66.2±0.5	1
WT+30μM PG	57.3±0.6	14
WT+70μM PG	25.5±1.4	62
WT +100μM PG	28.6±1.1	57
WT+70μM PG +9.3μM CL	8.4±1.2	88

Figure 3. ATPase Assays with aPLs for RecA and DNA Gyrase

(A) Anionic PLs inhibit DNA dependent ATP hydrolysis by RecA.

(B) Negative control with DNA gyrase DNA-dependent ATP hydrolysis indicates that the inhibition of RecA ATP hydrolysis is due to a specific interaction of anionic PLs with RecA.

(C) Titration of PG liposomes show that ATPase rates are inhibited as a function of concentration of PG.

(D) Absolute ATPase rates calculated from fits to the curves above. Error bars indicate SD.

See also Figure S3.

MG1655 and BKT29 after UV damage, associated with the periphery of the nucleoid (Figures 4E and 4J). RecA bundles in BKT29 appear morphologically distinct to those we observed in MG1655.

We also analyzed the localization of the ΔN10 and L2mut proteins in vivo using immunofluorescence (Figures S4A–S4D). Of the two mutants, L2mut cells had the largest decrease in polar RecA foci; however, this result may not be significant because both L2mut and ΔN10 showed very weak foci formation in vivo (<10% incidence). We tested whether weak foci formation is a result of alterations in protein expression by performing western blots of cell lysates expressing WT, L2mut, and ΔN10. L2mut and WT RecA expressed to similar levels, whereas ΔN10 expressed at 60%–70% of WT level (Figures S4E and S4F). The absence of foci in ΔN10 may be attributed to the decrease in DNA-less oligomers observed with mutations in this region (Eldin et al., 2000) or due to the slight decrease in protein expression. The involvement of L2 in the oligomeric states of RecA is less clear, however, mutations immediately flanking the L2-loop have been implicated in ATP binding and RecA oligomerization (Kelley and Knight, 1997; Logan et al., 1997).

Because ATPase activity within the RecA filament is required for filament disassembly and aPLs inhibited ATPase in vitro, we explored whether the slower rates of ATPase activity for membrane-associated RecA stabilized these structures in vivo. If correct, RecA-GFP foci in BKT29 cells should contain fewer RecA molecules than WT cells. We found the magnitude of the fluorescence intensity of RecA foci was significantly lower in BKT29 than in WT (Figure 4K), whereas strain UE53 showed no significant difference (Figure S7K). This suggests an increase in RecA turnover or a decrease in the accumulation of RecA in foci in the absence of PG and CL, which we probed using fluorescence recovery after photobleaching (FRAP) experiments in these cells (Movies S1 and S2). Approximately 60% of the RecA-GFP in WT, UE53, and BKT29 cells was dynamic (Figures 4L, S5A–S5D, and S7H), further indicating that RecA-GFP foci are not misfolded aggregates of protein in inclusion bodies that do not recover after photobleaching (Winkler et al., 2010). The recovery curves were composed of two distinct populations of molecules—a steep recovery by a fast-moving population (similar to free RecA diffusion) and a shallow recovery (faster than protein synthesis but slower than diffusion) characteristic of a reaction-dominant recovery (Figure S5C). In WT cells, ~26% of the RecA-GFP exchanged rapidly (Figures 4L and S5D), referred to as the fast-moving fraction (C_2), whereas in BKT29 cells C_2 was ~36% (Figures S5A, S5B, and S5D). C_2 had recovery kinetics and k_{off} values in the effective diffusion regime (Figures S5C and S5D), indicating that there were fewer free RecA-GFP molecules available in WT compared to BKT29. The remainder of the mobile RecA-GFP fraction in both strains corresponded to a slow-moving reaction-dominant fraction (C_1), which is significantly reduced in BKT29 (~21%) compared to WT (~37%) (Figures S5A, S5B, and S5D). C_1 also displayed drastically decreased k_{off} rates for BKT29 (0.001 s^{-1}) compared to WT (0.00011s^{-1})· Because the total percentage of recovered fluorescence does not vary significantly for both strains, the increase of free RecA in C_2 of BKT29 corresponds closely with the decrease of RecA in C_1. This relationship is also reflected in the ratio of k_{1on}/k_{1off} for BKT29 of 0.49 (Figure S5D), which indicates a high turnover rate of RecA within the C_1 fraction and release of these molecules into the free RecA pool. These observations support a model in which aPLs decrease the ATPase activity of RecA, stabilize the protein in a self-associated state, and promote the nucleation of RecA monomers.

aPLs Promote Stable and Efficient SOS Response

In vitro, LexA cleavage is efficient in the presence of extended RecA nucleoprotein filaments (Craig and Roberts, 1980). In vivo, Lesterlin et al. demonstrated that bundles of RecA form only after

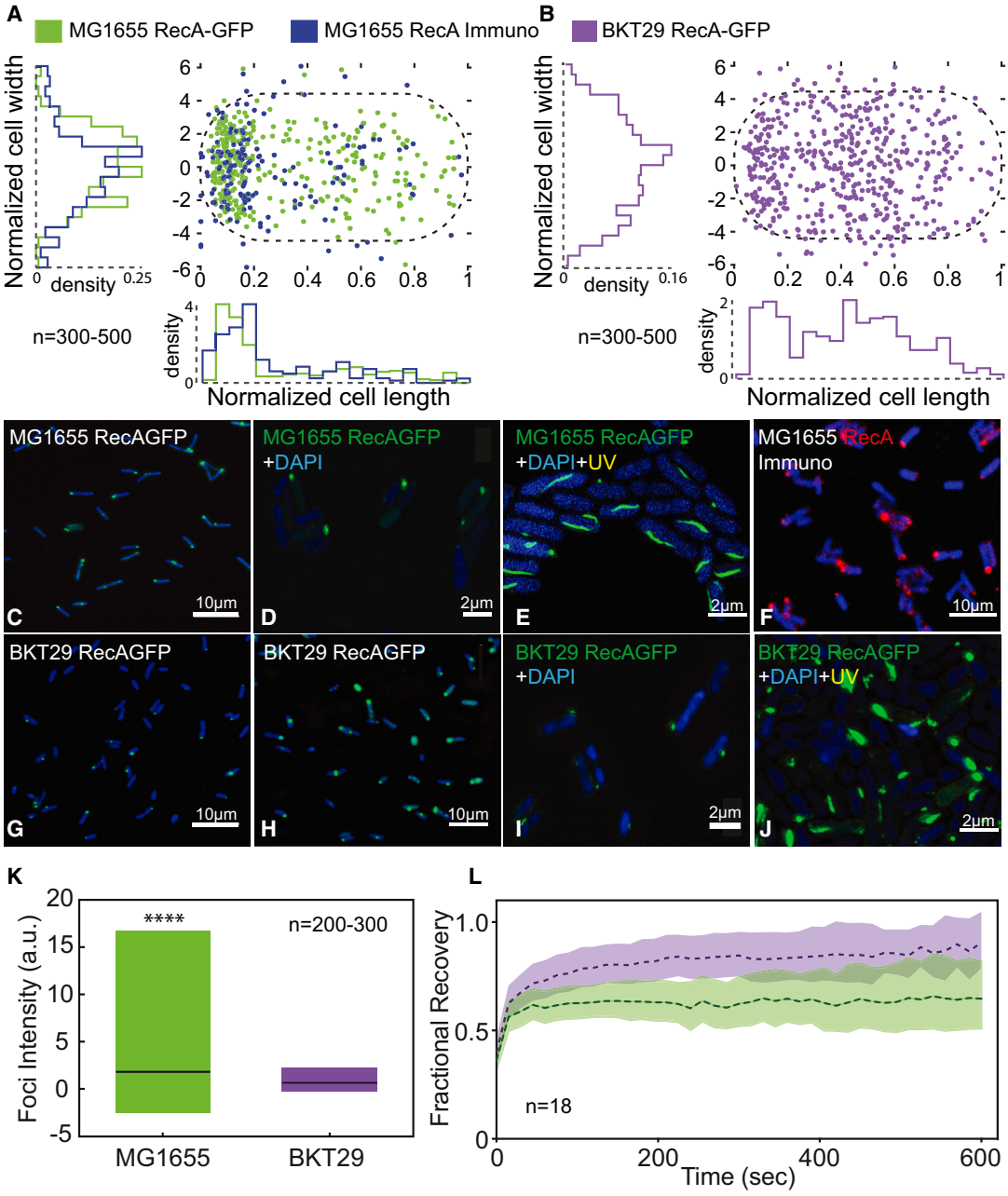


Figure 4. RecA Foci Localize to the Poles of *E. coli* and Mislocalize in the Absence of Anionic PLs

(A) Quantification of the position of RecA in WT cells using RecA-GFP and immunofluorescence labeling.

(B) RecA-GFP foci mislocalize in the absence of aPLs (strain BKT29).

(C) Representative image of RecA-GFP in WT cells (cells are falsely colored blue).

(D) 3D-SIM images show that RecA foci are located on the periphery of the nucleoid (depicted in blue by DAPI staining) in WT.

(E) We observe the formation of RecA filament bundles following UV treatment that were positioned proximal to the nucleoid.

(F) A representative image of immunofluorescence of RecA in WT cells.

(G–I) Representative images of RecA-GFP foci in BKT29 using epifluorescence microscopy (cells are falsely colored blue) (G and H) and 3D-SIM with DAPI (I).

(J) Images of UV-treated BKT29 cells using 3D-SIM and labeled with DAPI demonstrating short, ellipsoidal filament bundles.

(K) BKT29 cells have foci that display a significantly lower fluorescence intensity compared to WT. Plot displays distribution of foci intensity from min to max, with black line indicating mean. ****$p < 0.001$ calculated using a two-tailed t test.

(L) FRAP recovery curves for RecA-GFP foci for WT and BKT29. Shaded area indicates 95% CIs. BKT29 displays a larger mobile fraction of RecA compared to WT, indicating a higher turnover rate of protein within the foci. This result indicates that anionic PLs have a stabilizing effect on RecA within the cell.

See also Figures S4, S5, and S7.

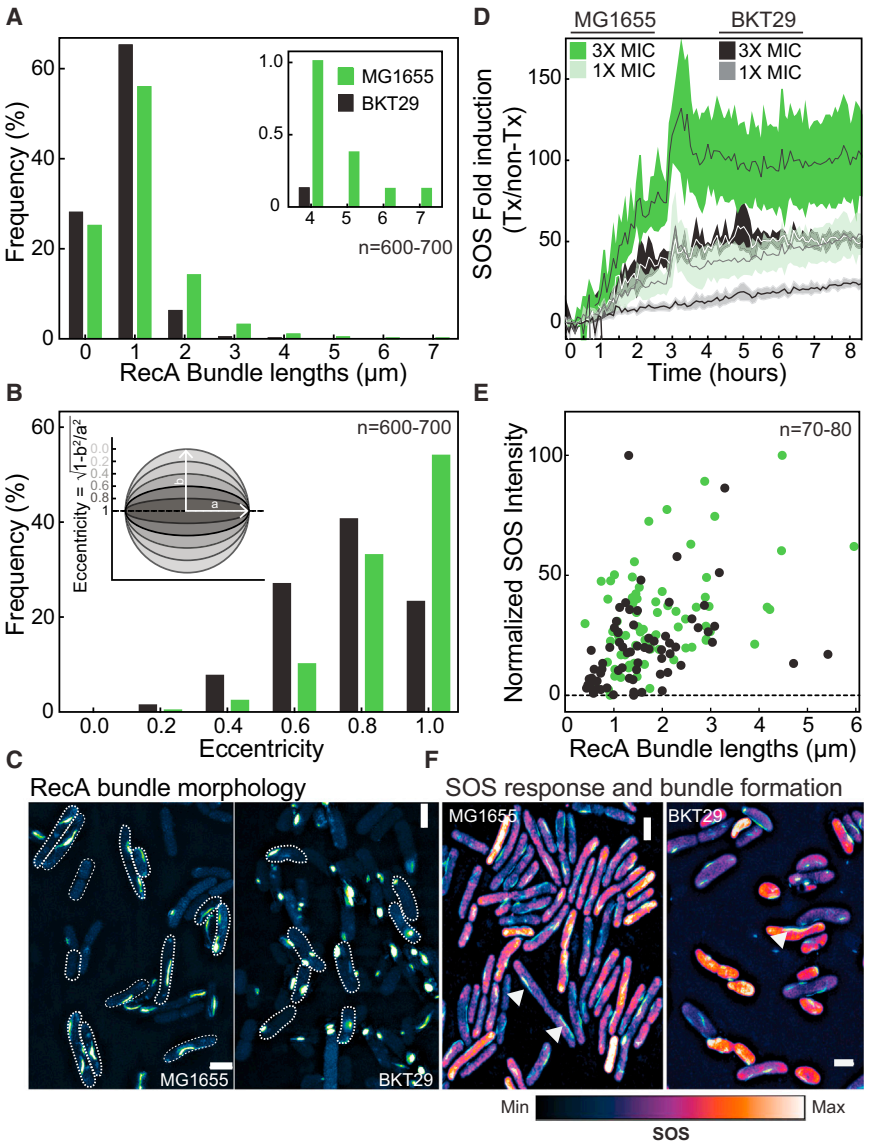


Figure 5. Analysis of SOS at a Single Cell Level in the Absence of Anionic PLs

(A) Measurement of RecA bundle lengths 1.5 hr after treatment with 1× MIC of norfloxacin shows that in WT (MG1655), >20% of bundles are >2 μm. These RecA bundles are 15% longer than in BKT29 in which ~85% RecA bundles are typically <1.5 μm.

(B) ~60% of bundles display a straight morphology (eccentricity = 1) in WT compared to ~20% in BKT29.

(C) Representative SIM images showing bundles in WT, and punctate, ellipsoidal RecA- GFP structures in BKT29.

(D) Using a *sulA*-promoter fusion to GFP, we observed that BKT29 has a reduced SOS response compared to WT when treated with 1× MIC of norfloxacin. This difference is also observed at 3× MIC. Shaded area represents SD of three biological replicates, with line and mean.

(E) The length of RecA bundles within the cell is positively correlated to the degree of SOS induced as observed by a *recN*-mCherry promoter fusion expressed with RecA-GFP. Shaded area indicates 95% CIs of a linear regression fit.

(F) Representative SIM image showing the overlay of SOS intensity with RecA bundles for WT and BKT29. White arrows indicate RecA bundles. Most cells show increased SOS (orange-white) when long bundles are present. The image displays the maximum intensity within one frame, which is a subset of the population of cells analyzed. Some outliers exist for BKT29 (seen in the accompanying images) in which short filaments have high levels of SOS and are visible in the plot. Because cells are also normalized by total area, longer cells with SOS intensities equal to shorter cells will have an overall higher SOS response. Cells that are blue indicate a lower level of SOS.

See also Figures S6 and S7.

DNA damage but are occluded from the nucleoid with approximately >85% of RecA within the bundles observed to be DNA-free. In this model, RecA proteins nucleate on exposed ssDNA at the site of damage and form a filament. This single filament is then sandwiched by multiple RecA filaments to produce bundles, which do not associate with DNA. It was also observed that RecA was not exchanged within these bundles suggesting that they are highly stable. A RecA mutant (E38K, K72R) that binds ssDNA and forms extended filaments but does not hydrolyze ATP, constitutively initiates the SOS response in vivo (Gruenig et al., 2008). This observation implies that RecA filaments that do not dissociate by hydrolyzing ATP are capable of producing an enhanced SOS response. We hypothesized that alterations in membrane composition will destabilize RecA filament bundles in vivo and affect the kinetics of the SOS response.

We analyzed the distribution of filament bundle lengths and morphology in WT and BKT29 cells using 3D-SIM (Figures 5A and 5C). We treated growing cell cultures with 10ng/mL norfloxacin (~1× minimal inhibitory concentration [MIC]) at 0.1–0.2 optical density and continued growth for a further 1.5 hr, after which cells were imaged. We found that WT and UE53 cells had a broad distribution of bundle lengths, with ~19% of bundles >2 μm long (Figures 5A and S7I). In BKT29 cells, only 6% of the bundles were >2 μm long with the longest bundles we observed being ~4 μm compared to 7 μm for WT cells (Figure 5A). We quantified bundle morphology in both strains using a metric for characterizing the deviation of bundle architecture from a sphere (eccentricity). Filament bundles that are spherical (i.e., foci-like) have an eccentricity of 0, whereas those that deviate away from a sphere (i.e., a straight line) have an eccentricity approaching 1. In BKT29 cells, bundles of all lengths were largely spherical and non-linear, unlike the morphology observed during DNA repair. Approximately 60% of all bundles in WT and UE53 cells were linear whereas only 20% of bundles were linear for BKT29 (Figures 5B and

S7G). Both the length and morphology analyses indicate that BKT29 is largely unable to form RecA filament bundles. This observation confirms the function of aPLs as a scaffold for the nucleation and stabilization of RecA bundles.

To test whether the inability to form RecA filament bundles affected the SOS response in BKT29, we used a plate-reader based assay and measured kinetics of SOS induction in strains of *E. coli* with WT RecA treated with 1X and 3X MIC norfloxacin (for WT, UE53, and BKT29) using a plasmid encoded copy of the SulA promoter located upstream of super-folder GFP (sfGFP). Norfloxacin produces DSBs that induce the SOS response and are repaired by RecA mediated recombination. We measured the fold increase of sfGFP expression from the *sulA* promoter in untreated and norfloxacin treated cells normalized by cell density, and observed a significant decrease in the amount of SOS induction after DNA damage in BKT29 cells (Figure 5D).

We also performed a survival analysis by monitoring colony-forming units after 3 hr of treatment with 10ng/mL norfloxacin. Approximately 60% of MG1655 RecA-GFP survived treatment whereas <5% of ΔrecA survived. MG1655 RecA-GFP is at least partially functional in repairing DSBs in the conditions that we tested (Figure S6A). Interestingly, BKT29 had lower survival compared to WT (~60%), confirming that these cells are impaired in repairing DNA damage. Defects in RecA-GFP foci and bundles were unique to BKT29 and did not appear in UE53, the parent strain of BKT29 that contains the suppressor mutations necessary for aPL deletion (Figures S7A–S7K).

We explored the possibility that the defect in RecA bundle formation in BKT29 may be the reason for the decreased SOS response observed in this strain. We monitored the level of SOS expression in WT and BKT29 at the single cell level while simultaneously measuring the lengths of RecA bundles formed. To obtain bundles of comparable lengths between WT and BKT29, we treated BKT29 with norfloxacin for an additional 1 hr (for a total of 2.5 hr). We found that the mean intensity of SOS observed in individual cells increased in proportion with bundle lengths observed for WT and BKT29 (Figures 5E and 5F). We determined the mean intensity by dividing the total intensity of each cell by the area and plotting it as a fraction of the maximum intensity observed within the population. This indicates BKT29 cells that eventually form long bundles are capable of producing the SOS response. However, BKT29 cells are slow to form RecA bundles with lengths comparable to those in WT cells and therefore display a decreased SOS response as a population.

DISCUSSION

The role of RecA in recombination repair is critical and during normal growth and replication, the nucleation of RecA on exposed ssDNA or double-stranded DNA can impede cellular processes. Our data are consistent with a model in which the IM stabilizes polymeric RecA structures at the poles and prevents its association with DNA during normal cellular growth and division. Induction of DNA damage (by UV or norfloxacin) redistributed RecA-GFP from the poles to the region of *E. coli* cells where the chromosome is located and where RecA formed visible bundles. The mechanisms underlying this process of RecA redistribution are currently unknown, but may be driven by the affinity of freely diffusing RecA to ssDNA.

CL and PG stabilize RecA structures without affecting the binding of ssDNA to RecA and altering its strand exchange activity in vitro. In contrast, CL and PG inhibited RecA ATPase significantly. ATPase is not required for RecA to catalyze strand pairing (Menetski et al., 1990); instead the hydrolysis of ATP has been appropriated to the disassembly of RecA filaments into monomers and facilitating strand pairing of heterologous chromosomal regions (Cox, 2007). Extended RecA nucleoprotein filaments are required for efficient SOS induction in vivo; however, ATPase is not required (Gruenig et al., 2008). These observations—framed within the context of the results presented in this study—imply that aPLs may also stabilize RecA bundles formed after the induction of DSBs by reducing the rate of ATPase within RecA filaments. In support of this hypothesis, we observed a dramatic decrease in the SOS response in cells lacking aPLs.

Our combined experimental and computational approach elucidated the membrane-binding domains in RecA. These regions are conserved across multiple species of bacterial RecA and mutational variation within these regions is infrequently tolerated in *E. coli* (Karlin and Brocchieri, 1996). The stringent conservation of amino acids in these positions has been attributed to the involvement of these regions in (1) strengthening the association between RecA monomers, and (2) interacting with ssDNA and catalyzing the hydrolysis of ATP. The placement of membrane-association domains of RecA at regions that are essential for its activity may provide a mechanism to reduce the probability that RecA will lose the ability to bind aPLs by genetic drift. The dominant-negative phenotype associated with mutations at these regions made it impossible for us to manipulate these regions to observe the effects of membrane association on DNA repair. Regardless, the positions of the membrane binding interfaces may provide insight into the modulation of ATPase activity within the RecA filament by aPLs. The N-terminal ten amino acids of RecA have been hypothesized to participate in monomer-monomer contacts important for polymerization. The N terminus (residues 1–33) has been suggested to play a role in RecA assembly-disassembly kinetics, specifically the coupling of a helix-coil transition in this region to RecA filament disassembly (Mikawa et al., 1995). Thus, stabilization provided by the membrane may prevent this structural transition and enable the formation of stable RecA bundles. Interestingly, *Bacillus subtilis* RecA—which possesses an N terminus that is not similar to *E. coli*—does not form RecA foci under normal growth, implicating the importance of this region for RecA self-association. The loop L2 (amino acids 195–209), and specifically F203 makes direct contact with ssDNA in vitro (Malkov and Camerini-Otero, 1995). Q194 and R196 are involved in catalyzing the hydrolysis of ATP. L2 has been demonstrated to mediate conformational changes associated with ATP binding to interaction with ssDNA and is subsequently involved in coupling DNA dependent ATPase to strand exchange. It is possible that inhibition of DNA dependent ATPase by aPLs occurs by blocking communication of the conformational changes associated with strand pairing by L2 to ATPase. Lesterlin et al. demonstrated that most of the RecA within bundles are not associated with

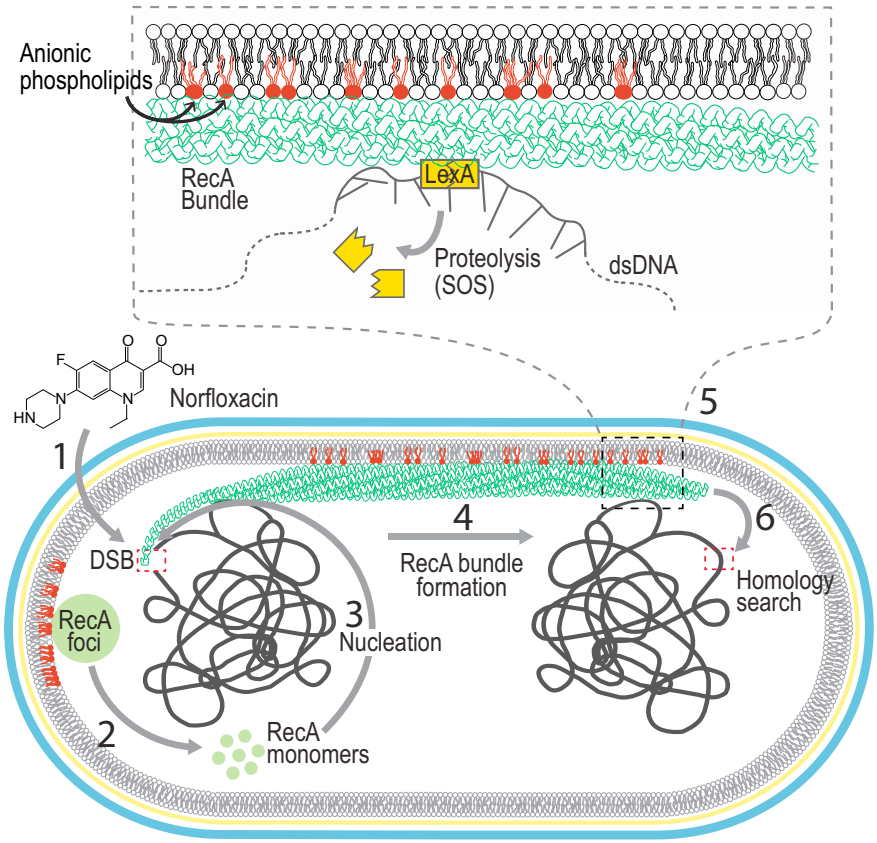


Figure 6. Model for the Role of the Inner Membrane in RecA Filament Bundle Formation

(1) Norfloxacin treatment of *E. coli* cells produces double-stranded breaks (DSBs). (2) RecA protein, which undergoes exchange between the cytoplasm and RecA foci, (3) nucleates on the processed DSB due to its high affinity to ssDNA (4) and forms RecA bundles associated with the IM (6), which extend across the cell searching for homology. (5) At some point during this search for homology, contact between the RecA bundle and LexA facilitates the autocleavage of LexA leading to the SOS response. RecA bundles are a stylized version of those observed by electron microscopy (Yu and Egelman, 1992).

DNA. This observation implies that the L2 loop is freely available for interaction with the IM when RecA is present as bundles.

To summarize, we have demonstrated that the IM is a key component for the nucleation and formation of RecA bundles in *E. coli*. We propose a model (Figure 6) in which RecA is nucleoid occluded and bound to aPLs at the poles of *E. coli* under normal conditions in storage structures that turn over at a constant rate. Damage to DNA that produces exposed ssDNA drives RecA nucleation due to high-affinity RecA-ssDNA interactions. ssDNA bound RecA produces filament bundles in an attempt to search for DNA homology using the IM as a scaffold for stability. This study sheds light on an exciting new dimension in RecA biochemistry and provides an example of yet another cytoplasmic protein that relies on its interaction with the bacterial membrane for spatial control of its activity and cellular function.

EXPERIMENTAL PROCEDURES

Strain Construction

E. coli strain BKT29 (*ΔaraBAD,rcsF::mini-Tn10cam,λ⁻, ΔclsABC, ΔymdB::kan, ΔpgsA,lpp-2*) was transformed with plasmid pCP20 (containing FLP recombinase) and grown overnight at 30°C to remove the kanamycin (kan) resistance cassette (kan^S). pCP20 was cured from strain BKT29 by growing at 43°C. To generate chromosomal RecA-GFP fusions, BKT29 kan^S, *E. coli* MG1655, and UE53 (*ΔaraBAD,rcsF::mini-Tn10cam,λ⁻,lpp-2*) were subjected to P1 transduction using a phage P1 lysate grown on strain ss3041 (*ygaD1::kan recAo1403 recA4136::gfp-901. recAo1403*). *recAo1403* refers to a single point mutation (T to A) in the operator/promoter region of *recA* that causes a 2-fold higher level of basal expression. *Gfp-901* refers to *mut-2* with the additional monomeric mutation A209T, which reduces aggregation that cause the formation of aberrant foci. For assays measuring SOS induction, plasmids pUA66-*sulA* promoter-GFP (*pSulA*-GFP), and pUA66-GFP were transformed into WT MG1655, UE53, and BKT29 kan^S. Plasmid *precN*-mCherry was constructed with a *recN* promoter fused to mCherry on a pBR322 backbone and transformed into BKT29 RecA-GFP and MG1655 RecA-GFP to monitor SOS. This plasmid was SOS-inducible under norfloxacin treatment (Figure S6B).

Quantifying RecA Binding to Liposomes by Measuring the Fluorescence Quenching of Tryptophan

To determine an apparent K_d of RecA to aPLs, we measured changes in the fluorescence intensity of Trp290 and 309 during the titration of RecA with liposomes. We fixed the excitation of a PTI Quantamaster 300 spectrofluorimeter at λ = 295 and collected fluorescence data at 37°C. We titrated liposomes consisting of 100% PC (negative control), 100% PG, 50%:50% PC:PE, and 80%:20% PC:CL into purified *E. coli* RecA (0.7 μM) in 1.4 ml of R buffer (see Supplemental Experimental Procedures) and mixed the suspension thoroughly using a pipette. We incubated mixtures for 5 min at 37°C and imaged the fluorescence emission by scanning from λ = 300–400 nm. We corrected

measurements of fluorescence intensity for the dilution of RecA during titration. We also accounted for scattering of light by liposomes and corrected our fluorescence measurements by subtracting values of fluorescence that we measured for liposome-only titrations into buffer. The titration of 100% PC liposomes into RecA did not produce an appreciable change in fluorescence intensity at λ = 300–400 nm, and thus we calculated the binding constants for PC:CL and PC:PE liposomes to RecA using only the concentration of CL or PE respectively. We calculated the fraction of RecA bound to liposomes using the equation: $B = (F_{adj} - F_{min})/(F_{max} - F_{min})$, where F_{adj} is the fluorescence intensity corrected for dilution and scattering, and F_{max} and F_{min} are the maximum and minimum fluorescence intensities we measured at λ = 320 nm. We calculated the free lipid concentrations for CL, PG, and PE using the equation: $[PL] = B \times [PL]_{total}$. We plotted the values we calculated for B against the free lipid concentration of CL, PG, and PE to obtain Langmuir binding isotherms and fit the data to the modified one-site specific binding equation: $Y = (B_{max} \times X^h)/(K_d{}^h + X^h)$.

Implicit Membrane Simulations

For the implicit membrane model, we use the generalized Born model with a simple switching function (GBSW) (Im et al., 2003), augmented with the Gouy-Chapman-Stern (GCS) model (Barrat and Hansen, 2003; Stern, 1924) for the anionic membrane surface. The salt concentration was set to 0.02 M NaCl, and parameters in the GCS model were chosen based a membrane with 27% PG and 73% PC. To identify favorable binding orientations, we performed a binding energy scan by rotating a rigid RecA monomer—constructed based on the crystal structure, PDB: 3CMT—with its center of mass fixed at 25 Å away from the membrane center. Guided by this binding energy surface (Figure 2A), we used 14 independent GBSW-GCS molecular dynamics trajectories (~10 ns each) without imposing any structural restraints on RecA. Each trajectory started with a different orientation. Some of the trajectories led to dissociation of RecA from the membrane surface, while the rest converged to two distinct binding conformations that featured similar binding interfaces (Figure 2B) and had different orientations of the C-terminal domain; we refer to these two orientations as the parallel (Figure 2C) and perpendicular (Figure 2D) binding conformations. These conformations were present in subsequent explicit membrane simulations on a timescale of ~110 ns.

We computed the binding free energies of the two binding conformations using the GBSW-GCS model and the thermodynamic cycle described recently (Zhang et al., 2014), which demonstrated that this methodology accurately predicts the binding free energy of peptides with membranes. We tested several mutants that were designed based on the observed RecA/membrane binding interface, which involves mainly the DNA binding loop L2 and the N-terminal helix; to a lesser extent, the C-terminal domain also contributes to binding in the parallel binding conformation. We computed the binding free energies of all of these mutants (Table 1).

For more information on experimental methods, please see the Supplemental Experimental Procedures.

SUPPLEMENTAL INFORMATION

Supplemental Information includes Supplemental Experimental Procedures, seven figures, three tables, and two movies and can be found with this article online at http://dx.doi.org/10.1016/j.molcel.2015.09.009.

ACKNOWLEDGMENTS

We thank Steven Sandler for *E. coli* strain ss3041 and Brandon Tan and Ziqiang Guan for *E. coli* strain BKT29. We are grateful to Angela Gruber, Anjon Audhya, Alessandro Senes, Elizabeth Wood, and Darrell McCaslin for input, experimental protocols, and reagents. 3D-SIM and confocal imaging were performed at the Biochemistry Optical Core. We acknowledge Dr. Elle Grevstad of the Biochemistry Optical Core (Department of Biochemistry, UW-Madison) for technical assistance. This research was supported by the National Science Foundation under grant no. DMR-1121288, NIH grant 1DP2OD008735-01 (to D.B.W.), NIH grant GM32335 (to M.M.C.), a Mao Wisconsin Distinguished Graduate Fellowship (to M.R.), and grants BIR-9512577 (National Science Foundation) and S10 RR13790 (NIH) (to the Biophysics Instrumentation Facility).

Received: May 13, 2015
Revised: August 14, 2015
Accepted: September 9, 2015
Published: October 15, 2015

REFERENCES

Barrat, J.-L., and Hansen, J.-P. (2003). Basic Concepts for Simple and Complex Liquids (Cambridge University Press).

Brenner, S.L., Zlotnick, A., and Griffith, J.D. (1988). RecA protein self-assembly. Multiple discrete aggregation states. J. Mol. Biol. *204*, 959–972.

Britt, R.L., Chitteni-Pattu, S., Page, A.N., and Cox, M.M. (2011). RecA K72R filament formation defects reveal an oligomeric RecA species involved in filament extension. J. Biol. Chem. *286*, 7830–7840.

Cox, M.M. (2007). Motoring along with the bacterial RecA protein. Nat. Rev. Mol. Cell Biol. *8*, 127–138.

Craig, N.L., and Roberts, J.W. (1980). E. coli recA protein-directed cleavage of phage lambda repressor requires polynucleotide. Nature *283*, 26–30.

Egelman, E.H., and Stasiak, A. (1988). Structure of helical RecA-DNA complexes. II. Local conformational changes visualized in bundles of RecA-ATP gamma S filaments. J. Mol. Biol. *200*, 329–349.

Eldin, S., Forget, A.L., Lindenmuth, D.M., Logan, K.M., and Knight, K.L. (2000). Mutations in the N-terminal region of RecA that disrupt the stability of free protein oligomers but not RecA-DNA complexes. J. Mol. Biol. *299*, 91–101.

Garvey, N., St John, A.C., and Witkin, E.M. (1985). Evidence for RecA protein association with the cell membrane and for changes in the levels of major outer membrane proteins in SOS-induced Escherichia coli cells. J. Bacteriol. *163*, 870–876.

Gruenig, M.C., Renzette, N., Long, E., Chitteni-Pattu, S., Inman, R.B., Cox, M.M., and Sandler, S.J. (2008). RecA-mediated SOS induction requires an extended filament conformation but no ATP hydrolysis. Mol. Microbiol. *69*, 1165–1179.

Im, W., Lee, M.S., and Brooks, C.L., 3rd (2003). Generalized born model with a simple smoothing function. J. Comput. Chem. *24*, 1691–1702.

Karlin, S., and Brocchieri, L. (1996). Evolutionary conservation of RecA genes in relation to protein structure and function. J. Bacteriol. *178*, 1881–1894.

Kelley, J.A., and Knight, K.L. (1997). Allosteric regulation of RecA protein function is mediated by Gln194. J. Biol. Chem. *272*, 25778–25782.

Kuvichkin, V.V., Danev, R.S., Shigematsu, H., and Nagayama, K. (2009). DNA-induced aggregation and fusion of phosphatidylcholine liposomes in the presence of multivalent cations observed by the cryo-TEM technique. J. Membr. Biol. *227*, 95–103.

Lesterlin, C., Ball, G., Schermelleh, L., and Sherratt, D.J. (2014). RecA bundles mediate homology pairing between distant sisters during DNA break repair. Nature *506*, 249–253.

Levin-Zaidman, S., Frenkiel-Krispin, D., Shimoni, E., Sabanay, I., Wolf, S.G., and Minsky, A. (2000). Ordered intracellular RecA-DNA assemblies: a potential site of in vivo RecA-mediated activities. Proc. Natl. Acad. Sci. USA *97*, 6791–6796.

Logan, K.M., Skiba, M.C., Eldin, S., and Knight, K.L. (1997). Mutant RecA proteins which form hexamer-sized oligomers. J. Mol. Biol. *266*, 306–316.

Malkov, V.A., and Camerini-Otero, R.D. (1995). Photocross-links between single-stranded DNA and Escherichia coli RecA protein map to loops L1 (amino acid residues 157-164) and L2 (amino acid residues 195-209). J. Biol. Chem. *270*, 30230–30233.

Menetski, J.P., and Kowalczykowski, S.C. (1985). Interaction of recA protein with single-stranded DNA. Quantitative aspects of binding affinity modulation by nucleotide cofactors. J. Mol. Biol. *181*, 281–295.

Menetski, J.P., Bear, D.G., and Kowalczykowski, S.C. (1990). Stable DNA heteroduplex formation catalyzed by the Escherichia coli RecA protein in the absence of ATP hydrolysis. Proc. Natl. Acad. Sci. USA *87*, 21–25.

Mikawa, T., Masui, R., Ogawa, T., Ogawa, H., and Kuramitsu, S. (1995). N-terminal 33 amino acid residues of Escherichia coli RecA protein contribute to its self-assembly. J. Mol. Biol. *250*, 471–483.

Oliver, P.M., Crooks, J.A., Leidl, M., Yoon, E.J., Saghatelian, A., and Weibel, D.B. (2014). Localization of anionic phospholipids in Escherichia coli cells. J. Bacteriol. *196*, 3386–3398.

Papanastasiou, M., Orfanoudaki, G., Koukaki, M., Kountourakis, N., Sardis, M.F., Aivaliotis, M., Karamanou, S., and Economou, A. (2013). The Escherichia coli peripheral inner membrane proteome. Mol. Cell. Proteomics *12*, 599–610.

Rajendram, M., Hurley, K.A., Foss, M.H., Thornton, K.M., Moore, J.T., Shaw, J.T., and Weibel, D.B. (2014). Gyramides prevent bacterial growth by inhibiting DNA gyrase and altering chromosome topology. ACS Chem. Biol. *9*, 1312–1319.

Renner, L.D., and Weibel, D.B. (2011). Cardiolipin microdomains localize to negatively curved regions of Escherichia coli membranes. Proc. Natl. Acad. Sci. USA *108*, 6264–6269.

Renzette, N., and Sandler, S.J. (2008). Requirements for ATP binding and hydrolysis in RecA function in Escherichia coli. Mol. Microbiol. *67*, 1347–1359.

Renzette, N., Gumlaw, N., Nordman, J.T., Krieger, M., Yeh, S.P., Long, E., Centore, R., Boonsombat, R., and Sandler, S.J. (2005). Localization of RecA in Escherichia coli K-12 using RecA-GFP. Mol. Microbiol. *57*, 1074–1085.

Stern, O. (1924). Zur theorie der elektrolytischen doppelschicht. Z Elektrochem Angew P *30*, 508–516.

Story, R.M., Weber, I.T., and Steitz, T.A. (1992). The structure of the E. coli recA protein monomer and polymer. Nature *355*, 318–325.

Tan, B.K., Bogdanov, M., Zhao, J., Dowhan, W., Raetz, C.R., and Guan, Z. (2012). Discovery of a cardiolipin synthase utilizing phosphatidylethanolamine and phosphatidylglycerol as substrates. Proc. Natl. Acad. Sci. USA *109*, 16504–16509.

Vivian, J.T., and Callis, P.R. (2001). Mechanisms of tryptophan fluorescence shifts in proteins. Biophys. J. *80*, 2093–2109.

Voloshin, O.N., Wang, L., and Camerini-Otero, R.D. (2000). The homologous pairing domain of RecA also mediates the allosteric regulation of DNA binding and ATP hydrolysis: a remarkable concentration of functional residues. J. Mol. Biol. *303*, 709–720.

Winkler, J., Seybert, A., König, L., Pruggnaller, S., Haselmann, U., Sourjik, V., Weiss, M., Frangakis, A.S., Mogk, A., and Bukau, B. (2010). Quantitative and spatio-temporal features of protein aggregation in Escherichia coli and consequences on protein quality control and cellular ageing. EMBO J. *29*, 910–923.

Yu, X., and Egelman, E.H. (1992). Direct visualization of dynamics and cooperative conformational changes within RecA filaments that appear to be associated with the hydrolysis of adenosine 5′-O-(3-thiotriphosphate). J. Mol. Biol. *225*, 193–216.

Zhang, L.L., Yethiraj, A., and Cui, Q. (2014). Free energy calculations for the peripheral binding of proteins/peptides to an anionic membrane. 1. Implicit Membrane Models. J. Chem. Theory Comput. *10*, 2845–2859.

Molecular Cell, Volume *60*

Supplemental Information

Anionic Phospholipids Stabilize RecA Filament Bundles in *Escherichia coli*

Manohary Rajendram, Leili Zhang, Bradley J. Reynolds, George K. Auer, Hannah H. Tuson, Khanh V. Ngo, Michael M. Cox, Arun Yethiraj, Qiang Cui, and Douglas B. Weibel

Figure S1. HMMM simulations, related to Figure 2. (A) 2 trajectories of RecA interacting with a membrane are projected onto the solvation PMF map. The trajectories start with red diamonds (filled and non-filled) and end with purple diamonds with a rainbow color scheme. We used the ending structure and solvated back in GBSW-GCS implicit membrane model. The orientation after 5 ns of simulations are shown in crossed circle for trajectory 1 and crossed diamond for trajectory 2. (B) Average insertion depth of RecA into the membrane calculated from these two trajectories. (C) Ending structure of trajectory 1, displaying the // orientation. (D) Ending structure of trajectory 2 displaying the ⊥ orientation. (E) Relative concentration of upper layer PS around the N-terminus of RecA during the 110 ns simulation on HMMM membrane. The scaled PS density is calculated using time averaged number of upper layer PS lipid around the N-terminus divided by the surrounding area times a factor of 14. The bin size for time is 14 ns and the bin size for distance is 7 Å.

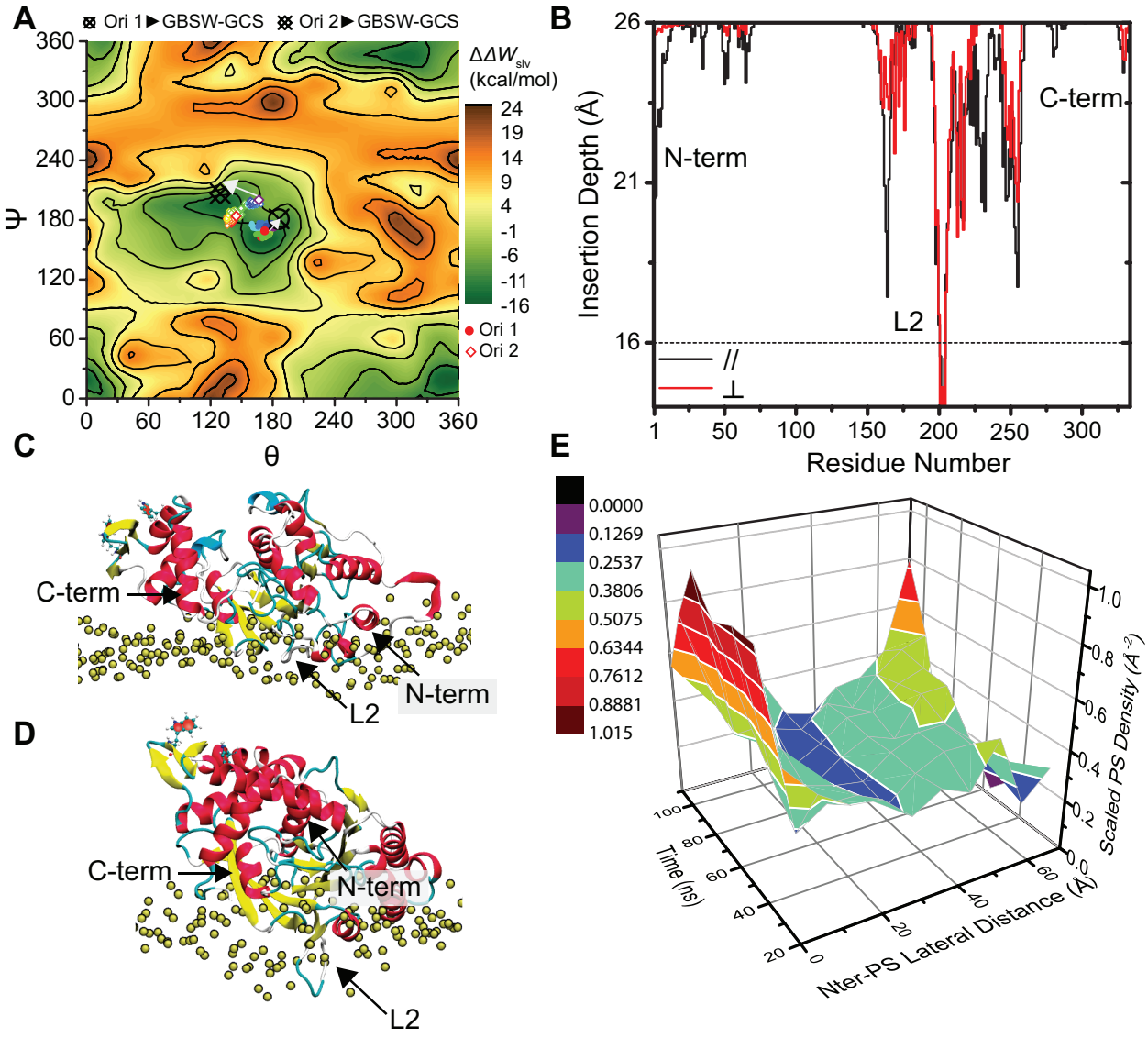

A
Ori 1►GBSW-GCS
Ori 2►GBSW-GCS
ΔΔW_slv (kcal/mol)
24
19
14
9
4
-1
-6
-11
-16
Ori 1
Ori 2
Ψ
θ
B
Insertion Depth (Å)
N-term
C-term
L2
//
⊥
Residue Number
C
C-term
N-term
L2
D
C-term
N-term
L2
E
0.0000
0.1269
0.2537
0.3806
0.5075
0.6344
0.7612
0.8881
1.015
Time (ns)
Nter-PS Lateral Distance (Å)
Scaled PS Density (Å^-2)

Figure S1

Figure S2. Comparison of the circular dichroism spectra of WT RecA with L2Mut and ΔN10RecA, related to Figure 2. (A) The baseline-subtracted values of the CD spectra were converted to mean residue molar ellipticity (θ_{MR}) using the equation $\theta_{MR}=100\times\theta/(CMR\times l)$, where CMR refers to Mean Residue Concentration and l refers to path length of the cuvette. This demonstrates that WT RecA, L2Mut and ΔN10RecA have comparable structural properties and their overall structures are quite similar. The slight change in the ellipiticity value for L2Mut may be the result of variations in protein concentration. GuHCl titrations at the indicated concentrations of GuHCl for (B) L2mut, (C) N10 and (D) WT RecA in the presence of 70μM PG liposomes (dashed lines) and in the absence of liposomes (filled lines).

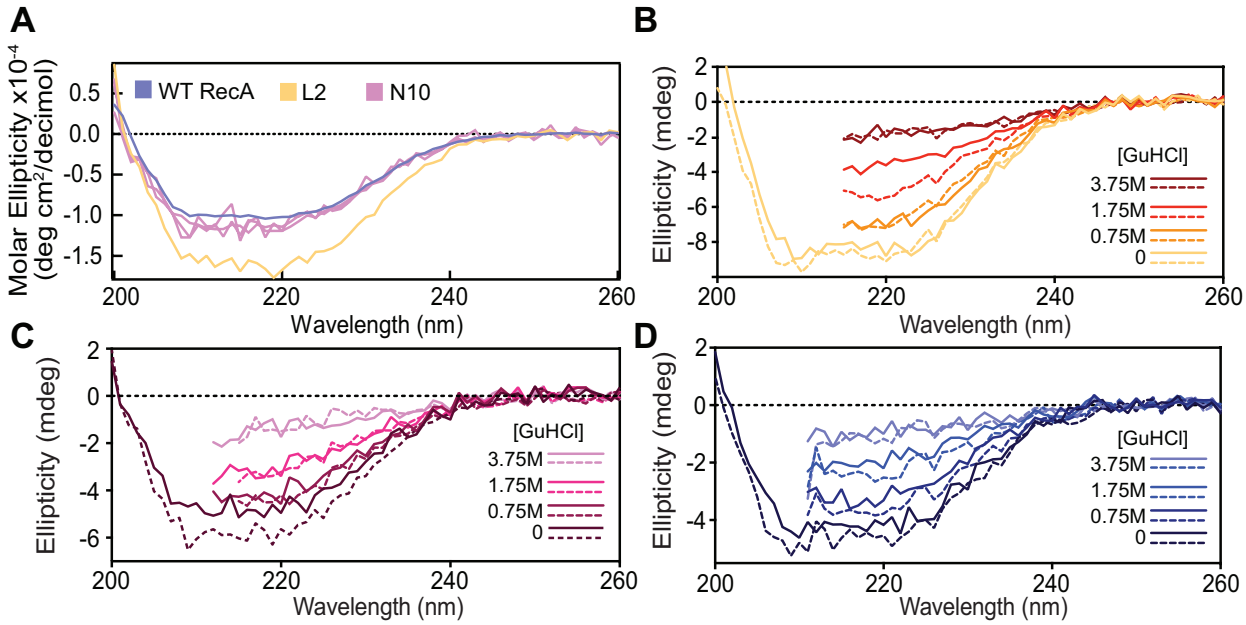
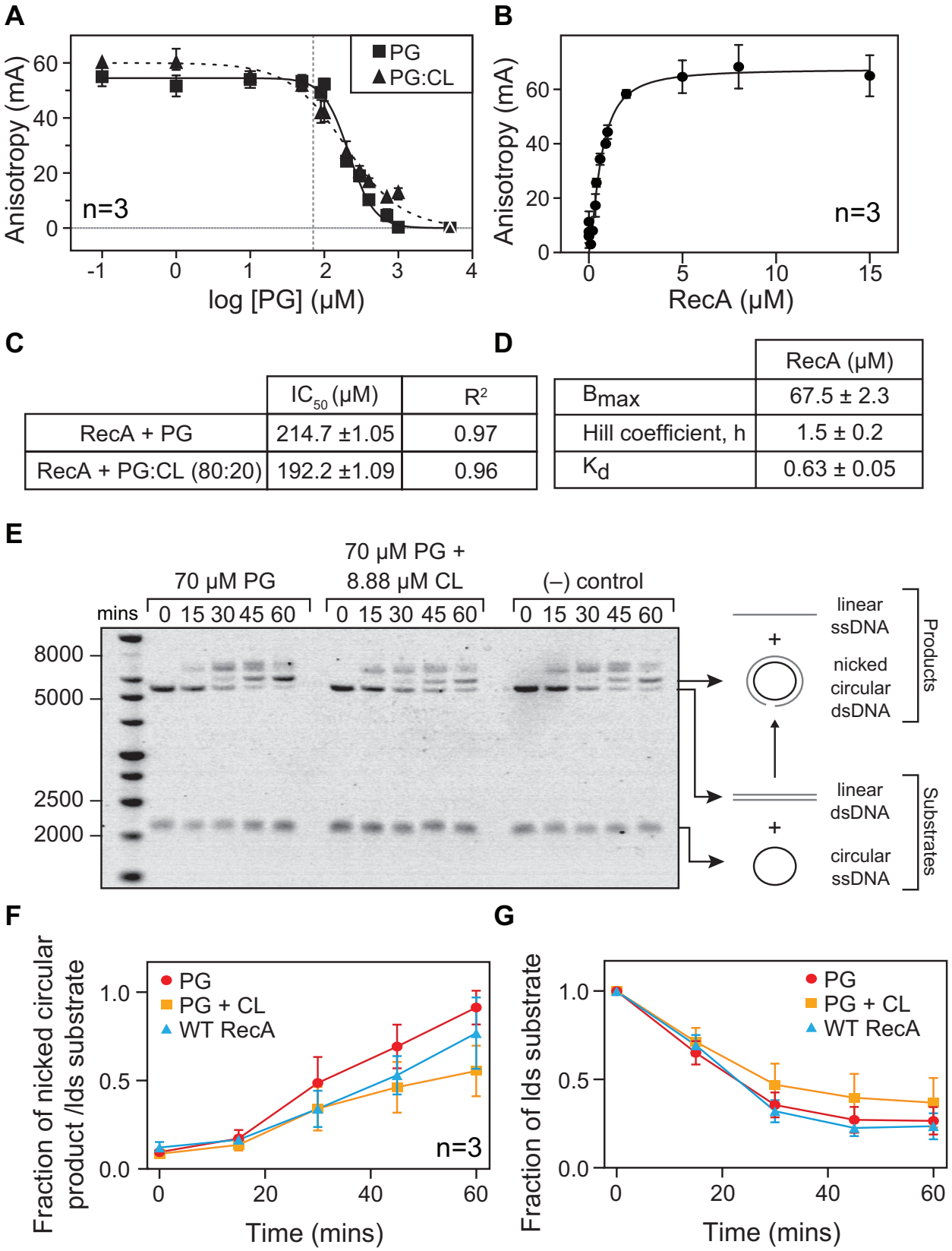

A
B
C
D
WT RecA
L2
N10
Molar Ellipticity x10⁻⁴
(deg cm²/decimol)
Ellipticity (mdeg)
Wavelength (nm)
[GuHCl]
3.75M
1.75M
0.75M
0

Figure S2

Figure S3. ssDNA binding and in vitro strand exchange assays for RecA in the presence of aPLs, related to Figure 3. (A and C) IC50 experiments showing the decrease in fluorescence anisotropy with titrations of PG or PG:CL containing liposomes. Dashed line indicates concentration of aPLs at which ssDNA binding is perturbed. The IC50 is high, indicating that PG or CL do not compete with ssDNA for binding with RecA. (B and D) Fluorescence anisotropy measurements of the binding affinity of RecA to ssDNA confirm a high affinity, cooperative association of RecA with ssDNA (Hill coefficient >1). (E) A representative strand exchange gel that was used to quantify the formation of nicked circular product. (F) Quantification of the nicked circular product formed as a fraction of the linear double-stranded (lds) substrate as a result of strand exchange by RecA. The difference in the amount of product formed is not significant in the presence of anionic PLs indicating that PG/CL do not inhibit RecA mediated recombination in vitro. (G) Quantification of the disappearance of the lds substrate as a function of time confirms that RecA performs strand exchange at a comparable rate in the presence of PG and CL and that substrates are not trapped in an intermediate state before the formation of nicked circular product. All error bars indicate SD.



	IC_{50} (μM)	R^2
RecA + PG	214.7 ±1.05	0.97
RecA + PG:CL (80:20)	192.2 ±1.09	0.96

	RecA (μM)
B_{max}	67.5 ± 2.3
Hill coefficient, h	1.5 ± 0.2
K_d	0.63 ± 0.05

Figure S3

Figure S4. Analysis of L2mut and N10 immunofluorescence, related to Figure 4.

Localization of (A) L2 and (B) N10 RecA fused to an Xpress epitope tag. Both mutants display less than 10% foci. Cells are false colored blue with red RecA punctae. (C and D) The positioning of these foci within the cells appears to not be concentrated at the poles. (E) Cell lysates, normalized by total protein were analyzed by western blotting with anti-Xpress antibody towards WT RecA, L2Mut and N10. (F) The resulting bands were quantified using Image J and expressed as a percentage of WT RecA.

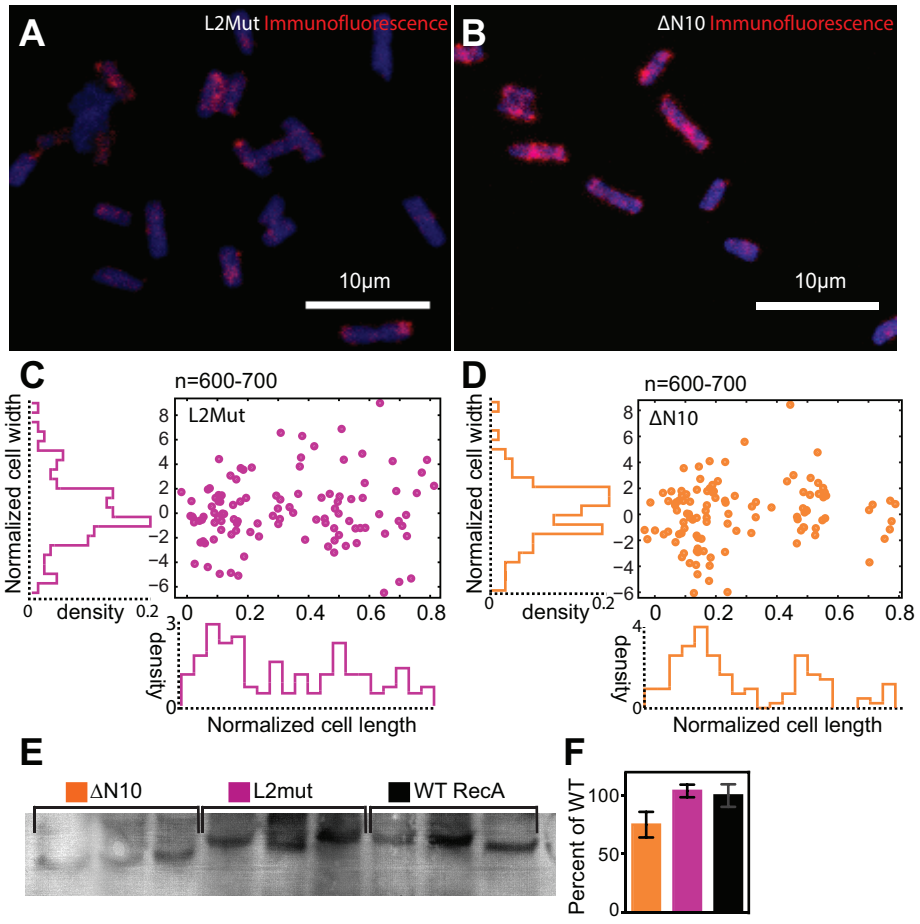
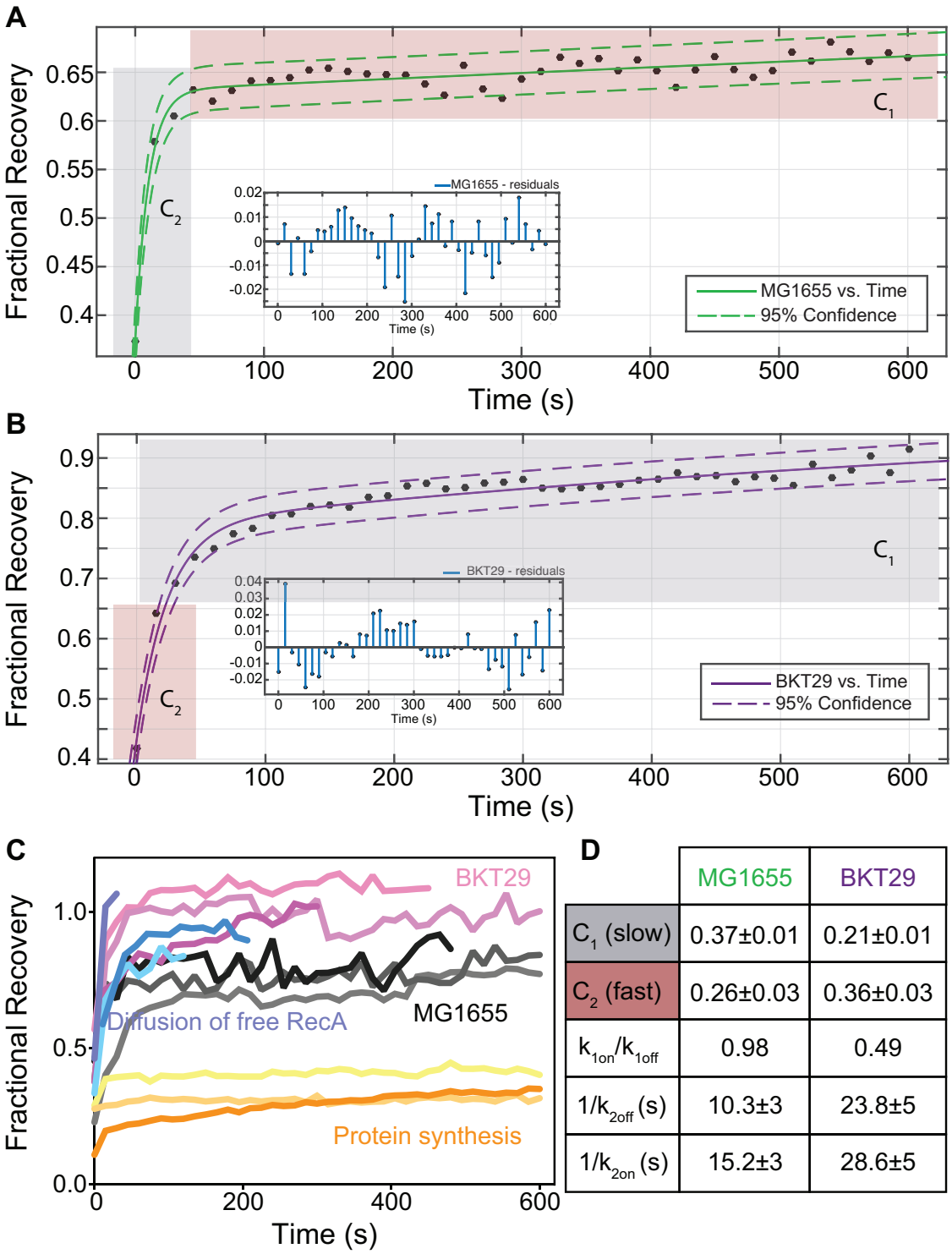

A
L2Mut Immunofluorescence
10μm
B
ΔN10 Immunofluorescence
10μm
C
n=600-700
L2Mut
Normalized cell width
density
Normalized cell length
D
n=600-700
ΔN10
Normalized cell width
density
Normalized cell length
E
ΔN10
L2mut
WT RecA
F
Percent of WT

Figure S4

Figure S5. FRAP analysis for WT and BKT29, related to Figure 4. Double exponential fit and plot of residuals of FRAP using an equation for approximating a two-state binding model for (A) MG1655 (R^2=0.95) and (B) BKT29 (R^2=0.97). Dashed line indicates the 95% confidence intervals for fits. Gray and pink boxes represent the slow (C_1) and fast (C_2) fractions. (C) Three independent recovery curves for diffusion of free RecA (light blue-dark blue), protein synthesis (yellow-orange), BKT29 (pink-purple), and MG1655 (gray-black) observed within *E. coli* cells. For the FRAP curves for protein synthesis, the whole cell was bleached and recovery was monitored every 15 s. FRAP curves for diffusion of free RecA was observed by bleaching cytoplasmic RecA not associated with foci. (D) Table of estimated parameters obtained from double-exponential fits. Gray and pink boxes represent the slow (C_1) and fast (C_2) fractions.



D

	MG1655	BKT29
C_1 (slow)	0.37±0.01	0.21±0.01
C_2 (fast)	0.26±0.03	0.36±0.03
k_{1on}/k_{1off}	0.98	0.49
$1/k_{2off}$ (s)	10.3±3	23.8±5
$1/k_{2on}$ (s)	15.2±3	28.6±5

Figure S5

Figure S6. Survival assays, related to Figure 5. (A) Measurement of % survival when treated with norfloxacin at 1xMIC for 3 h. MG1655 RecA-GFP is able to partially recover under DNA damage. Interestingly, BKT29 is impaired in the ability to recover after DNA damage confirming a role for aPLs in DNA repair/SOS. Error bars indicate SD. (B) Control for recN-promoter fusion with mcherry constructed in this study, showing that it is inducible under the DNA damage conditions used for monitoring SOS intensity using SIM. BKT29 containing this promoter also shows decreased SOS response as observed in Fig.5D indicating that both *sulA* and *recN* promoters are induced to a lesser degree in BKT29. Bars are min to max fold induction with black line at mean.

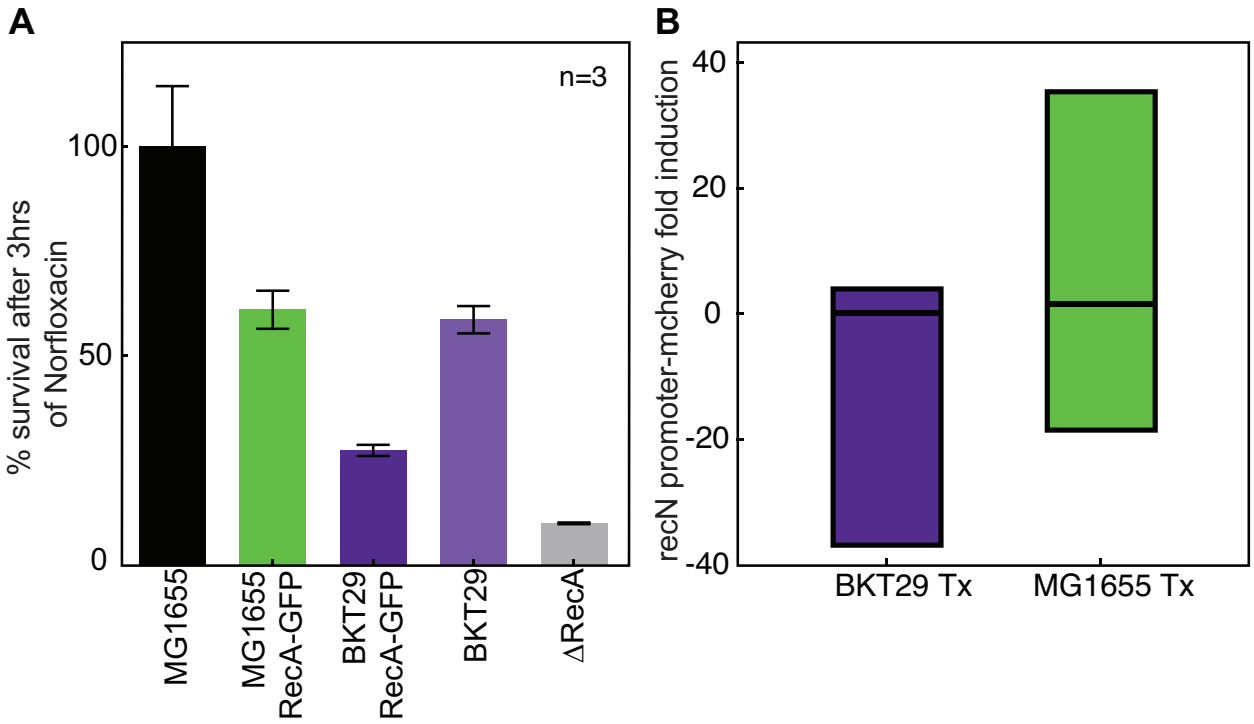

A
n=3
% survival after 3hrs of Norfloxacin
100
50
0
MG1655
MG1655 RecA-GFP
BKT29 RecA-GFP
BKT29
ΔRecA
B
recN promoter-mcherry fold induction
40
20
0
-20
-40
BKT29 Tx
MG1655 Tx

Figure S6

Figure S7. Strain UE53 shows similar localization, bundle morphology and SOS to WT, related to Figure 4,5. Controls showing that UE53 (parent strain containing the suppressor mutations that arose during anionic PL deletion) shows no significant deficiencies in (A,E) localization, (B,C,G and I) RecA bundle morphology, (D and F) bundle length versus SOS response in single cells ,(H) foci turnover (error reflects 95% confidence intervals), (J) SOS response (min to max fold induction with black line at mean for 3 biological replicates) and (K) foci intensity (error bars reflect SD), compared to WT.

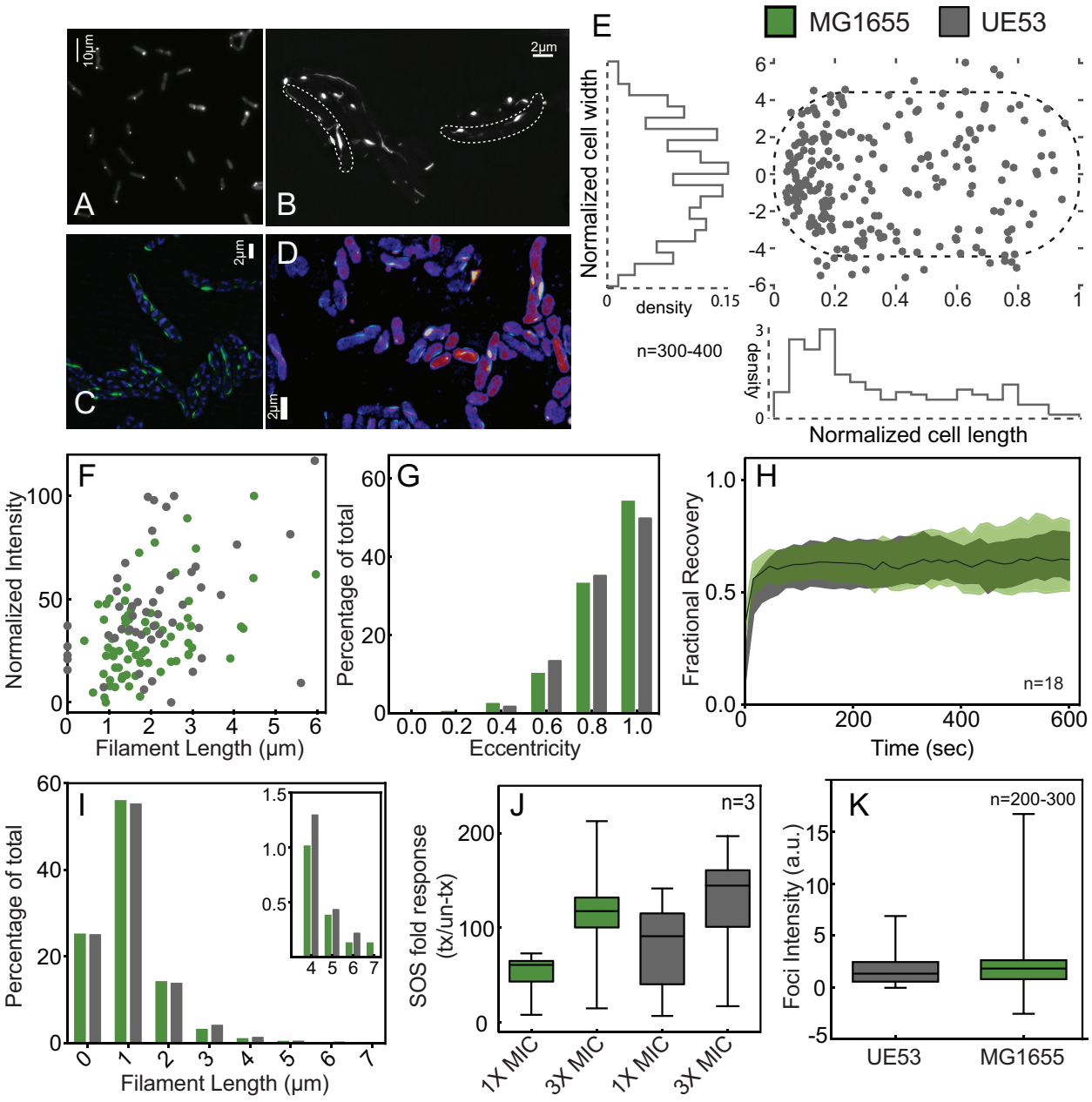

A
10μm
B
2μm
C
2μm
D
2μm
E
MG1655
UE53
Normalized cell width
density
n=300-400
density
Normalized cell length
F
Normalized Intensity
Filament Length (μm)
G
Percentage of total
Eccentricity
H
Fractional Recovery
n=18
Time (sec)
I
Percentage of total
Filament Length (μm)
J
n=3
SOS fold response (tx/un-tx)
1X MIC
3X MIC
1X MIC
3X MIC
K
n=200-300
Foci Intensity (a.u.)
UE53
MG1655

Figure S7

Table S1. Parameters of L2Mut and Δ10RecA binding to PG and CL, related to Figure 2.

Lipid	Protein	K_d (μM)	Hill Coefficient	R^2
PG	ΔN10RecA	>45	n.d	0.92
	L2MutRecA	>45	n.d	0.91
	WT RecA	17.3±3	2.2	0.96
CL	ΔN10RecA	>13	n.d	0.78
	L2MutRecA	>18	n.d	0.74
	WT RecA	3.2±0.7	1.9	0.84

Table S2. Phenotypes observed for mutations of conserved amino acids within the *E. coli* RecA protein, related to Figure 2.

	Recombination[a]	**Coprotease**[a]
Δ N9	Rec−	n.d
I195A	Rec−	n.d
R196A	Rec−	n.d
K198A	Rec−⋆	n.d
I199A	Rec−	n.d
V201A	Rec±	n.d
F203A	Rec−⋆	n.d

[a] adapted from (McGrew and Knight, 2003). ⋆ indicates proficiency for λ recombination activity but not for DNA repair.

Table S3. Size estimates of liposomes using dynamic light scattering, related to Figure 1 and Figure 2.

Liposome Formulations	Particle size (nm)	Polydispersity Index
100% PG	84.6±30.52	0.152±0.019
80:20% PG:CL	160.6±58	0±0.017
100% PC	112±33.56	0±0.015
90:10% PC:CL	106.3±38.03	0±0.009
80:20% PC:CL	114.8±43.26	0±0.012
70:30% PC:CL	118.2±41.36	0±0.01

Supplemental Experimental Procedures

Protein Purification. 1) *Purification of recombinant E. coli RecA*. We used a nuclease-deficient E. coli strain RDK1896 (exoI $^{-}$ exoIII $^{-}$ endoI $^{-}$ recJ $^{-}$) co-transformed with plasmids pAIR79 (containing the E. coli WT RecA protein under a T7 promoter) and pT7POL26 (containing T7 RNA polymerase under a lac promoter) to purify E. coli RecA. The purification procedure contained an additional size exclusion step. 2) *Purificaiton of ΔN10 and L2mut.* We used *E. coli* BL21.DE3 transformed with pET28b (containing ΔN10 or L2mut under a T7 promoter) to purify ΔN10 and L2mut versions of RecA. Cultures were grown to an absorbance of 0.6 (λ = 600 nm) and induced with 1 mM IPTG for 4 h at 37 °C. Cells were pelleted by centrifugation at 4000xg for 20 min at 4 °C. Pellets were flash-frozen in liquid nitrogen. Flash frozen pellets were thawed on ice and lysis buffer (50 mM NaH_2PO_4, 300 mM NaCl, 10mM Imidazole, pH 8) (5X the mass of the pellet) was added. Lysozyme (L6876, from Sigma Aldrich, St. Louis, MO) was added to a final concentration of 5 mg/mL and was stirred for 1 h at 4 °C. The resulting cell suspension was sonicated and centrifuged at 10,000xg for 30 min at 4 °C. The supernatant was mixed with Ni-NTA agarose (Qiagen, Valencia, CA) and incubated with shaking at 4 °C for 1 h. The mixture was loaded in a column and washed 2X with wash buffer (50mM NaH_2PO_4, 300mM NaCl, 20mM Imidazole, pH 8). The column was eluted with elution buffer (50 mM NaH_2PO_4, 300 mM NaCl, 250 mM Imidazole, pH 8). The fractions were pooled and dialyzed using a 20Kda cut-off dialyzer cassette

(ThermoScientific, Rockford, IL) into R buffer and concentrated using a spin column (Vivaspin GE, Pittsburgh, PA). The resulting protein concentrate was subjected to thrombin (Biotinylated Thrombin, Millipore, Billerica, MA) cleavage with a dilution factor for thrombin of 1:200 for 4 h at 25 °C. To remove biotinylated thrombin, 25 μL of streptavidin agarose beads were added to the reaction mix and slowly rotated at 25 °C for 1.5 h. This mixture was added to a spin filter (Millipore, Billerica, MA) and centrifuged at 500xg for 10 min. To remove undigested protein, 25 μL of Ni-NTA resin was added to the resulting flow-through and incubated at 25 °C for 30-45 min with gentle agitation. The Ni-NTA resin was spun down in a spin filter (Millipore, Billerica, MA) @ 500xg for 10 min.

We determined the concentration of RecA by measuring the absorbance at λ=280 nm and corrected for scattering at λ=320 nm. We used the molar extinction coefficient of 2.23×10^{-4} M^{-1} cm^{-1}. Purified RecA was stored in R buffer (20 mM Tris-HCl, 0.1 mM EDTA, pH 7.4). We verified that purified *E. coli* RecA did not contain exonuclease and endonuclease activity and established the purity of RecA by mass spectrometry.

Preparation of liposomes. We used lipids from Avanti Polar Lipids (Alabaster, AL): 1,2-di-(9Z-octadecenoyl)-*sn*-glycero-d-phospho-(1'-*rac*-glycerol) (DOPG; herein referred to as PG), 1,2-di-(9Z-octadecenoyl)-*sn*-glycero-d-phosphocoline (DOPC; herein referred

to as PC), 1,2-di-(9Z-octadecenoyl)-*sn*-glycero-3-phosphoethanolamine (DOPE; herein referred to as PE) and 1,1′,2,2′-tetra-(9Z-octadecenoyl) cardiolipin (CL). To create liposomes, we dried aliquots of the mixtures of the lipids dissolved in chloroform in a glass vial under argon, and removed traces of solvent by incubating in a vacuum chamber for 12-15 h at 25 °C. We resuspended the dried lipid fractions in R buffer and sonicated (Branson 2510 bath sonicator) the suspensions for 20 min. We immersed the vials containing the lipids in liquid nitrogen for ~2 min and sonicated for 20 min. We repeated the sonication step in liquid nitrogen 3 times. To prepare liposomes of the lipid mixtures, we extruded sonicated suspensions of lipids (Avanti Polar Lipid Mini Extruder) through a membrane containing 0.1-μm pores. We used the following compositions of liposomes in this study: 100% PC, 100% PG, 95:5% PC:CL, 90:10% PC:CL, 80:20% PC:CL, 70:30% PC:CL, 80:20% PC:PE, 80:20% PC:PG and 80:20% PG:CL. All ratios reflect weight percentages unless otherwise mentioned. We characterized liposomes using dynamic light scattering and confirmed their monodispersity (Table S3). As liposomes consisting of 100% CL are unstable due to the physical attributes of CL, we performed all experiments with CL using mixtures containing PC or PG. PC forms aggregates with DNA in the presence of Mg^{2+} ions (Kuvichkin, 2009). Many of the RecA assays we performed require Mg^{2+} ions, such as the strand exchange, ATPase, and ssDNA binding assays, and thus we avoided using liposomes containing PC in these experiments.

Co-flotation assays of RecA and liposomes. We incubated wild type RecA (17.3 μM) for 5 min at 37 °C with liposomes containing one of five different PL compositions: 0.5 mM PC (100% PC); 0.5 mM PC and 13.8 μM CL (95:5% PC:CL); 0.47 mM PC and 27.5 μM CL (90:10% PC:CL); 0.42 mM PC and 55.1 μM CL (80:20% PC:CL); and 0.37 mM PC and 82.7 μM CL (70:30% PC:CL). We mixed reactions with an 80% solution of Accudenz® (Accurate Chemical and Scientific Corporation, Westbury, NY) in 125 mM HEPES, 500 mM KCl, and 50% glycerol. We pipetted the resulting mixture (40% Accudenz) into a 500 μL Beckman Coulter polycarbonate ultracentrifuge tube. We created a density gradient by successively layering 35%, 30%, and 0% Accudenz® solutions and centrifuged the tubes at 281,227 x g at 4 °C for 2 h using a Beckman Coulter Optima Max-XP tabletop ultracentrifuge with a TLA 120.1 rotor. After centrifugation, we harvested 20 μL of liquid from the top layer, performed electrophoresis of equal volumes of the harvested material on a denaturing polyacrylamide gel (SDS-PAGE), and stained the gel using the SilverQuest™ Silver Staining Kit (Life Technologies, Grand Island, NY). We imaged gels using a FOTODYNE® Gel Documentation system (Hartland, WI) and quantified the intensity of the bands in ImageJ (version 1.43u). We also performed this experiment with PC:PE (80:20%) and PC:PG (80:20%). The concentrations of the lipids were 0.25 mM PC and 0.07 mM PE; 0.26 mM PC and 0.07 mM PG. We ran 100% PC controls at concentrations of 0.25-0.26 mM to test for non-specific binding to PC.

Explicit membrane simulations with the HMMM model. Lipid mixing is difficult to sample adequately using conventional explicit membrane simulations, especially in the presence of protein binding. Therefore, we have adopted the highly mobile membrane-mimetic (HMMM) model (Ohkubo et al., 2012) in which the membrane tails are truncated and replaced by an organic solvent 1,1-dichloroethane (DCLE). The initial orientations of RecA protein are taken from the GBSW-GCS simulations. The protein was solvated with water and placed on a 68:252 phosphatidylserine (PS):PC membrane within the HMMM model. We neutralized the system with 0.02 M NaCl. Simulations were carried out with NAMD for 110 ns. To maintain the area per lipid in the HMMM, we used the NPAT ensemble with constant pressure coupling for the z direction at 1 atm. The average box size is approximately 110×110×110 $Å^3$.

The projection of the HMMM trajectories on the binding energy map (Fig S1A) suggests that these simulations lead to similar binding conformations as the GBSW-GCS calculations discussed in the main text. This result is further confirmed by the analysis of residues on the binding interface (Fig S1B) and snapshots from the trajectories, which illustrate the parallel (Fig S1C) and perpendicular (Fig S1D) binding conformations of RecA on the binding. Compared to the two binding conformations from the GBSW-GCS simulations (Fig 2C-D in the main text), the perpendicular conformation in the HMMM simulations is more tilted such that the C-terminal domain lies closer to the membrane;

in the parallel binding conformation, the N-terminal helix is less associated with the membrane. Loop L2 is observed to insert deeper into the membrane in the HMMM simulations than in the GBSW-GCS trajectories. Moreover, the HMMM simulations clearly illustrate that the binding of the N-terminal helix leads to a notable local enhancement of anionic lipid concentration (Fig S1E). The heterogeneous lipid distribution is clearly not captured in the implicit membrane simulations and may account for some of the quantitative differences between the results of the HMMM and GBSW-GCS simulations. Nevertheless, the general significance of the N-terminal helix and loop L2 to membrane binding is consistently captured in both the implicit and explicit membrane simulations, supporting the robustness of our prediction of the membrane binding interface.

Assaying the ATPase activity of RecA. We used a spectrophotometric coupled enzyme assay to measure the DNA-dependent ATPase activity of recombinant *E. coli* RecA in the presence of liposomes (100% PG or 80:20% PG:CL). We coupled the regeneration of ATP from phosphoenolpyruvate (PEP) and ADP to the oxidation of NADH and measured the decrease in the absorbance of light at 37 °C using a Varian Cary 300 dual beam spectrophotometer (λ_{em}=380 nm). We set the cell path length and band pass to 1 cm and 2 nm, respectively. Using the NADH extinction coefficient (1.21 mM^{-1} cm^{-1} at λ=380 nm), we converted the oxidation of NADH to the hydrolysis of ATP. Linear fits

were used to obtain steady-state rates of ATP hydrolysis. Reaction mixtures (100 μL) contained 1 mM DTT, 3.5 mM phosphoenolpyruvate, 10 U/mL pyruvate kinase (PK), 10 U/mL lactate dehydrogenase (LDH), 1.5 mM NADH, 8 μM of circular single stranded DNA (concentration reflects total nucleotides), 3 μM RecA, 5 mM ATP, 0.8 μM of recombinant *E. coli* SSB in RecA activity buffer (25 mM Tris-OAc (pH 7.4), 1 mM DTT, 3 mM potassium glutamate, 10 mM $Mg(OAc)_2$, and 5% glycerol (w/v)). After pre-incubation of the reaction mixture containing either 100% PG liposomes (at indicated lipid concentrations) or 80:20% PG:CL liposomes (at a final lipid concentration of 70 μM PG and 9.25 μM CL) for 10 min at 37 °C, ATP and SSB were added to start the reaction.

DNA Gyrase ATPase assay. ATPase assays with *E. coli* DNA gyrase (New England Biolabs, Ipswich, MA) were performed as described previously (Rajendram et al., 2014). Briefly, reaction mixtures (80 μL) contained 35 mM Tris-HCl, 24 mM KCl, 4 mM $MgCl_2$, 2 mM DTT, 5 mM spermidine, and 6.5% (v/v) glycerol at pH 7.5. We added 3.5 mM PEP (Alfa Aesar), pyruvate kinase (PK; 10 U) (MP Biomedicals), lactate dehydrogenase (LDH; 10 U) (MP Biomedicals), 1.5 mM NADH (Acros organics), 1 U of DNA gyrase and liposomes at concentrations indicated above were preincubated for 10 minutes at 37°C. ATP (Fisher Scientific) was added to start the reaction. Rates of ATP hydrolysis were calculated as described above.

Fluorescence polarization measurements of RecA-ssDNA binding. We used a 50-nt 3′ fluorescein labeled oligomer (Integrated DNA Technology, Coralville, IA) with the following sequence: 5′-GGC CTC GCG GTA GCT GAG CTC GGA GCG CAC GAT TCG CAC TGC TGA TGT TC-3′ to perform fluorescence polarization measurements as described previously (Britt et al., 2011). To prevent dissociation of RecA from ssDNA, we performed measurements in the presence of the non-hydrolyzable ATP analog, AMPPNP. For FP experiments, the reaction consisted of 25 mM tris acetate (pH 7.8), 10 mM magnesium acetate, 3 mM potassium glutamate, 5% w/v glycerol, 1 mM dithiothreitol (DTT), and 3 mM AMPPNP. We serially diluted RecA into the storage buffer, added fluorescent oligonucleotide at a final concentration of 10 nM, and incubated the solution in the absence of light for 20 min at 37 °C. Each dilution was performed in triplicate. We performed measurements in a TECAN infinite M1000 multiwell plate reader and corrected anisotropy values for the G-factor of the instrument and the fluorophore (fluorescein) of the tagged ssDNA. Using the binding isotherm obtained from the above procedure as a guide, we chose to use a fixed concentration of RecA (3 μM) with the components mentioned above for IC50 experiments. We titrated liposomes at increasing aPL concentrations into 3μm RecA until the anisotropy was reduced to a baseline value. IC50 was calculated as the amount of aPLs required to reduce the anisotropy to 50% of untreated values using Graphpad Prism version 6.0e.

RecA-catalyzed three-strand DNA exchange assays. Homologous λ-phage ΦX174 circular single stranded DNA (cssDNA) and double stranded DNA (dsDNA) was from New England Biolabs (Ipswich, MA). We digested dsDNA using the restriction enzyme XhoI and purified the resulting linear dsDNA (ldsDNA) using a Qiagen purification kit. We performed three-strand DNA exchange assays (reaction volume, 60 μL) in RecA activity buffer consisting of 25 mM Tris-OAc (pH 7.4), 1 mM DTT, 3 mM potassium glutamate, 10 mM $Mg(OAc)_2$, 5% glycerol (w/v), and a coupled enzyme ATP regeneration system consisting of pyruvate kinase (PK, 10 units/mL) and phosphoenolpyruvate (PEP, 2 mM). After addition of 10 μM of total nucleotides (nt) of cssDNA substrate, we added RecA (3 μM) along with liposomes—100% PG liposomes at a final lipid concentration of 70 μM, and 80:20% PG:CL liposomes at a concentration of 70 μM PG and 8.8 μM CL) and incubated the mixture at 37 °C for 10 min. We chose this concentration of PG because it is 10x the apparent K_d we determined from binding experiments. The final CL concentration of liposomes was regulated by the largest weight percent of CL that we could dope into PG to form stable liposomes. We were able to make stable liposomes consisting of a composition of 80% PG and 20% CL. We added ATP (3 mM) and single stranded DNA binding protein (SSB) (3 μM; Promega, Madison, WI) and incubated the reaction for 10 min to equilibrate. We initiated the reaction by adding ldsDNA (10 μM of nt). We removed aliquots of the reaction (10 μL) at 0, 15, 30, 45, and 60 min and incubated them for 15 min in quenching solution

consisting of 15% Ficoll, 0.24% bromophenol blue, and 4% SDS. We analyzed the products of the reaction by separating them on a 0.8% agarose gel containing ethidium bromide using electrophoresis at 20 mA. Gels were imaged using FOTODYNE® Gel Documentation system (Hartland, WI) and quantified using Fiji (version 2.00-rc-30/1.49s).

CD Spectroscopy. Measurements of CD spectra were performed on an AVIV Model 420 CD Spectrometer (Aviv Biomedical, Lakewood, NJ), in a fixed path-length cuvette of 1mm. Protein concentrations were determined as described previously, diluted in R Buffer and CD spectra were acquired at a fixed temperature of 37°C. For GuHCl titratrations, an 8M stock solution of GuHCl (Thermo Scientific, Rockford, IL) was diluted at the indicated concentrations, into protein samples at 1.4μM. Protein samples were made with 25X R Buffer, so that when different volumes of GuHCl are added, the salt concentrations remain identical. The final volume of each titration was 300 μLs. The samples were incubated for 20 minutes at room temperature and CD spectra were recorded at 37°C. The same cuvette was utilized for subsequent titrations to avoid baseline shifts. CD spectrum of R Buffer was subtracted from that of each titration to perform baseline corrections.

Microscopy of RecA-GFP.

Epifluorescence. MG1655 RecA-GFP, UE53 RecA-GFP and BKT29 RecA-GFP were grown at 37 °C with shaking at 200 rpm until they reach mid-log phase (absorbance of 0.5-0.6 at λ=595 nm) in M9 supplemented minimal media consisting of 1X M9 salts (12.8g $Na_2HPO_4.7H_2O$, 3g KH_2PO_4, 0.5g NaCl, 1g NH_4Cl in 1L), 0.4% glycerol, 0.2% casamino acids, 2 mM $MgSO_4$, and 0.1 mM $CaCl_2$. We placed a suspension of cells (5 μL) on a glass coverslip and positioned an agarose pad (2% w/v) on top of the cells. We imaged cells using both phase contrast and epifluorescence using a Nikon TE2000-E inverted microscope equipped with an Andor iXon EMCCD (Belfast, Northern Ireland). Samples were illuminated with a 120W mercury arc lamp (X-cite Series 120, EXFO, Mississauga, Ontario Canada) and images were acquired using a 100X objective, a 500/20x excitation filter, and a 535/30nm emission filter. All data was collected with the shutter off and a 100 ms exposure time controlled by Metamorph software (version 7.5.6.0 MDS Analytical Technologies, Downington, PA).

Confocal. FRAP experiments were performed on a Nikon A1R+ Confocal system with galvano scanning enabled to achieve high resolution imaging on a 100X oil objective. The 488nm laser was used for photobleaching with a pulse at 10% laser intensity for 20 ~1s loops. Recovery was observed at 15s intervals until pre-bleach intensities were achieved or until the curve flat-lines. Cultures were grown as described for epifluorescence microscopy and spotted on an agarose pad.

Structured Illumination Microscopy (SIM). We performed 3D-SIM using a Nikon N-SIM microscope with a 100X oil objective and acquired multiple z-stacks at a step size of 0.15μm increments to capture the entire volume of the cell. The images were reconstructed using default reconstruction parameters built into the Nikon N-SIM NIS Elements software (version 4.0). Reconstructed images were further processed using Fiji (version 2.00-rc-30/1.49s) to obtain the max-intensity Z projection. These projections were then analyzed using MATLAB's ImageSegmenter and Image Region Analyzer modules to obtain RecA bundle lengths and eccentricity parameters. To correlate SOS response to bundle lengths, we utilized a *recN* promoter fused to mCherry and imaged both RecA-GFP and subsequently mCherry fluorescence using the SIM. mCherry was imaged in a single z-plane. RecA bundle lengths were again characterized using a combination of the ImageSegmenter and Image Region Analyzer MATLAB modules. mCherry fluorescence was corrected for background using Fiji and the mean intensity for each cell was calculated by drawing an ROI around each cell. To obtain normalized intensities, the highest intensity in each dataset was considered to be 100 and 0 intensity units was considered 0.

Strains and growth conditions for immunofluorescence. RecA gene was amplified from *E. coli* MG1655 using primers containing a C-terminal epitope tag-Xpress™ DLYDDDDK. This gene was cloned into the pBAD33-C280 plasmid at sphI sites using

Gibson assembly (New England Biolabs, Ipswich, MA). The resulting plasmid was mutagenized using the Agilent QuikChange Site-Directed Mutagenesis kit (Agilent Technologies, Santa Clara,CA) to include the N10 and L2 mutations described in the main text. The resulting three WT-Xpress, ΔN10-Xpress and L2mut-Xpress pBAD plasmids were transformed into WT-MG1655. Cells were grown overnight in 30μg/mL chloramphenicol and the resulting cultures were subcultured into fresh LB. At ~0.1 O.D, 10mM arabinose is added to induce expression of tagged proteins and let grow for another 2.5 hours.

Immunofluorescence. 1mL of culture was centrifuged at 3000 rpm for 5 mins at 25°C. *Fixation.* The supernatant was removed and the resulting pellet was resuspended in 2.8% formaldehyde (Sigma Aldrich Corporation, St. Louis, MO) +0.04% glutaraldehyde (Fisher Scientific, Waltham, MA) in PBS (pH 7.0). The cells were fixed for 15 mins and centrifuged at 3000 rpm for 5 mins. *Lysozyme treatment.* Cells were washed twice with PBS and resuspended in TE buffer (10mM Tris-HCl, 1mM EDTA, pH 8.0) with 10μg/mL lysozyme (L6876, from Sigma Aldrich, St. Louis, MO) and incubated for 5 mins at 25°C. *Blocking.* Cells were spun down and washed twice in PBS+0.5% Tween 20 (PBST), resuspended in PBST+1% BSA (ChemCruz Biochemicals, Dallas, TX) and incubated 30 mins at 25°C. *Primary Antibody.* 5μg/mL of mouse anti-Xpress™ antibody (Life Technologies, Grand Island, NY) was applied and incubated at 4°C for 15 mins

followed by incubation at 25°C for 1.25 hrs. After incubation, cells were spun down and resuspended in 1mL of PBST+1% BSA. *Secondary Antibody.* 3µls of Alexa Fluor 488 goat anti mouse IgG (H+L) (Life Technologies, Grand Island, NY) was added to 150 µLs of resuspended cells and incubated in dark at 25°C for 15 mins. Cells were washed once with PBST and imaged using epifluorescence microscopy. Images were analyzed as described below.

Western Blotting. Cultures were grown and treated with IPTG in the same manner as for immunofluorescence. 1mL of each culture was harvested; cells were pelleted by centrifugation at 3000xg, flash frozen in liquid nitrogen and stored at -80°C till further analysis. Cells were thawed on ice, and lysed using FastBreak™ Cell Lysis Reagent (Promega Corporation, Madison, WI). Lysates were spun down at 16,000xg and supernatants were collected. Protein estimation was performed using the Pierce™ Microplate BCA Protein Assay Kit (RockFord, IL) with relevant BSA standards. We mixed samples 1:4 with Laemmli sample buffer (Bio-Rad, Hercules, CA) and performed electrophoresis on a 12.5% polyacrylamide gel (Bio-Rad). Proteins were transferred to nitrocellulose for 1 h at 100 V. The nitrocellulose was rinsed several times with dH_2O and blocked overnight at 4 ºC in 5% BSA in TBST buffer (20 mM Tris, 137 mM NaCl, 1% v/v Tween-20, pH 7.6). Blots were washed 2 × 5 min in TBST buffer. We diluted mouse anti-Xpress™ primary antibody 1:1,500 in in TBST buffer containing 5% BSA, incubated

the blots for 1 hour, and washed the blots 2 × 5 min in TBST buffer. We diluted a goat anti-mouse IgG secondary antibody conjugated to horseradish peroxidase (HRP) 1:4,000 in 2.5% BSA in TBST buffer, and incubated blots in this solution for 1 h. Blots were washed 2 × 5 min in TBST buffer, the surface of each blot was incubated in ECL Plus reagent (GE Healthcare) for 2 min, and blots were imaged using the ECL Plus setting on a Typhoon FLA 900 scanner (GE Healthcare). We quantified band volumes using ImageQuant (GE Healthcare).

MicrobeTracker analysis of polar localization. To quantitatively determine the localization of RecA in cells for fluorescence and immunofluorescence images, we used the MATLAB-based image analysis tool, MicrobeTracker (Sliusarenko et al., 2011). We used phase images to determine the perimeter of cells and superimposed the resulting meshes on the corresponding fluorescence images. We used SpotFinderZ to count localized foci of RecA-GFP within each cell. We segmented the cells (typically 36 segments per cell with a width of ~ 1 pixel) and determined which segments contained all or part of a RecA-GFP focus. We determined the percentage of all foci in each segment using the total number of foci identified in the population of cells, and plotted the results against the relative cell length to quantitatively illustrate protein localization. In a typical experiment we analyzed ~350 cells at each time point. To ensure that we were not biasing measurements, we segmented all cells within each frame unless there

were ambiguities that would influence the analysis, such as cells too close to the edges of a frame or cells clustered tightly together. Foci positions were plotted as a scatter function of two co-ordinates along the normalized segment length and normalized segment width using MATLAB. The intensities of all foci were also obtained using spotFinderZ and plotted using GraphPad Prism version 6.0.

FRAP analysis. Intensity information from FRAP images for pre- and post-bleach of whole cell (I_{WC}) and ROI (region of interest) (I_{ROI}) were obtained using Fiji. Because the diameter of the pinhole is larger than the ROI area and a majority of RecA intensity is accumulated in foci, bleaching of >20% of the RecA population occurs. This depletion of RecA due to bleaching a significant population of molecules will affect recovery. To account for this, normalization was performed as follows: $(I_{ROI})\times\{(I_{WC})_{t0}/(I_{WC})\}$ where I_{WCt0} refers to the pre-bleach intensity. After normalization, I_{ROIt}/I_{ROIt0} gives the fractional recovery of fluorescence after bleaching. This fractional recovery is plotted as a function of time and double-exponential curves were fit using MATLAB's curve-fitting module. Based on the shape of the recovery curve which was composed of two separate recovery regimes, a sharp recovery and a slow recovery, two equations were considered (Eq. 1) $frap\ (t)=1-C_1e^{-kofft}$ and (Eq. 2) $frap\ (t)=1-C_1e^{-k1offt}-C_2e^{-k2offt}$ where C_1 and C_2 are the equilibrium fractions of 'bound' complex and k_{1off} and k_{2off} refers to the equilibrium off-rate for C_1 and C_2 respectively (Sprague et al., 2004). In our system, 'bound' refers to

RecA that is present as polar foci. Both these solutions consider the presence of a reaction-dominant recovery regime based on a process slower than effective diffusion of free RecA. Best fits for our data were obtained with equation 2, which indicated the presence of two separate 'bound' fractions of RecA within foci. The ratio of k_{on}/k_{off} for C_1 and C_2 were solved for by using the following algebraic equations- $1/C_1=1+k_{1off}/k_{1on}$ $(1+k_{2on}/k_{2off})$ and $1/C_2=1+k_{2off}/k_{2on}$ $(1+k_{1on}/k_{1off})$.

Measurement of SOS using promoter-fusion assays. WT MG1655, UE53, and BKT29 kan^S strains containing *pSulA*-GFP and pUA66 were grown in lysogeny broth (LB) consisting of 1% (w/v) tryptone, 0.5% (w/v) yeast extract, and 0.5% NaCl (w/v) at 37 °C with shaking at 200 rpm overnight. 2 μL of overnight culture was diluted into 200 μL of LB and LB containing 10 ng/mL norfloxacin (1x the minimum inhibitory concentration). Absorbance was measured at λ=595 nm and GFP fluorescence was measured at λ_{Ex}= 485 nm and λ_{Em}= 515 nm using an Infinite® M1000 plate Reader (TECAN Systems, Inc., San Jose, CA). Analysis of SOS induction was performed after subtracting background from both absorbance and fluorescence measurements at time 0. The background corrected fluorescence values for each strain were corrected for basal GFP expression by subtracting values of pUA66 from *pSulA*-GFP. The resultant fluorescence values were divided by absorbance at each time point, t (*pSulA*-GFP Fluorescence (t)/Absorbance(t)).

The normalized values were compared such that fold SOS induction for norfloxacin-treated cultures were obtained from $(pSulA\text{-GFP/OD})_{treated}/(pSulA\text{-GFP/OD})_{untreated}$.

Survival Assays. Three independent cultures of MG1655, ΔRecA, MG1655-RecAGFP, BKT29 RecA-GFP and BKT29 were grown for 16hrs from three separate colonies at 37°C and 200 rpm shaking. These were subcultured 1:100 into 6mLs of LB. All cultures were staggered in time to account for different growth rates such that treatment with 10ng/mL of norfloxacin was possible at ~0.15-0.2 OD. 50μL aliquots of each culture were taken at time 0 and time 3hrs after treatment and were serially diluted into 450μLs of PBS and cells were plated on LB-agar plates. Plates were incubated at 37°C for 18 hrs and colonies were counted to obtain % survival relative to MG1655.

References

Bennett, C.H. (1976). Efficient Estimation of Free-Energy Differences from Monte-Carlo Data. J Comput Phys *22*, 245-268.

Britt, R.L., Chitteni-Pattu, S., Page, A.N., and Cox, M.M. (2011). RecA K72R filament formation defects reveal an oligomeric RecA species involved in filament extension. J Biol Chem *286*, 7830-7840.

Kuvichkin, V.V. (2009). Investigation of ternary complexes: DNA-phosphatidylcholine liposomes-Mg2+ by freeze-fracture method and their role in the formation of some cell structures. J Membr Biol *231*, 29-34.

McGrew, D.A., and Knight, K.L. (2003). Molecular design and functional organization of the RecA protein. Crit Rev Biochem Mol Biol *38*, 385-432.

Ohkubo, Y.Z., Pogorelov, T.V., Arcario, M.J., Christensen, G.A., and Tajkhorshid, E. (2012). Accelerating Membrane Insertion of Peripheral Proteins with a Novel Membrane Mimetic Model. Biophys J *102*, 2130-2139.

Rajendram, M., Hurley, K.A., Foss, M.H., Thornton, K.M., Moore, J.T., Shaw, J.T., and Weibel, D.B. (2014). Gyramides prevent bacterial growth by inhibiting DNA gyrase and altering chromosome topology. ACS Chem Biol *9*, 1312-1319.

Sliusarenko, O., Heinritz, J., Emonet, T., and Jacobs-Wagner, C. (2011). High-throughput, subpixel precision analysis of bacterial morphogenesis and intracellular spatio-temporal dynamics. Mol Microbiol *80*, 612-627.

Sprague, B.L., Pego, R.L., Stavreva, D.A., and McNally, J.G. (2004). Analysis of binding reactions by fluorescence recovery after photobleaching. Biophys J *86*, 3473-3495.

Zhang, L.L., Yethiraj, A., and Cui, Q. (2014). Free Energy Calculations for the Peripheral Binding of Proteins/Peptides to an Anionic Membrane. 1. Implicit Membrane Models. J Chem Theory Comput *10*, 2845-2859.